Transportation Research Part C 77 (2017) 495–515

Contents lists available at ScienceDirect

Transportation Research Part C

journal homepage: www.elsevier.com/locate/trc

Coordinated distributed adaptive perimeter control for large-scale urban road networks

Jack Haddad *, Boris Mirkin

Technion–Israel Institute of Technology, Faculty of Civil and Environmental Engineering, Technion Sustainable Mobility and Robust Transportation (T-SMART) Laboratory, Israel

ARTICLE INFO

Article history:
Received 20 March 2016
Received in revised form 27 October 2016
Accepted 5 December 2016
Available online 7 March 2017

Keywords:
Macroscopic fundamental diagram
Perimeter control
Distributed adaptive control

ABSTRACT

Perimeter traffic control for large-scale urban road networks has been studied by several researchers during the last decade. Recently, the initial steps towards taking into account model's uncertainties under control synthesis were made in Haddad and Shraiber (2014) and Haddad (2015), where by considering one- and multi- region control problem, respectively, a robust perimeter control has been designed to systematically take into account uncertainties in MFD-based dynamics, e.g. the MFD scatter. The robust control design can provide a fixed controller with constant gains to compensate all uncertainties, following the worst case scenario concept. In this paper, an adaptive control scheme is developed. Similarly to robust control, the developed adaptive control scheme postulates one controller structure, however, the controllers' gains vary with time to adapt themselves against the model parameter uncertainties.

In this paper, in order to accommodate uncertainties and take into consideration the restrictions on the available information, we deal with the adaptive perimeter control problem for multi-region MFD systems, which have an interconnected structure composing several homogeneous regions. Unlike previous works that assume centralized approach, where feedback informations are needed from all urban regions, in this paper we follow a coordinated distributed control approach, where regional control laws are developed depending on (i) real on-line local information of the region, i.e. regional accumulation and its perimeter control input only, and (ii) reference signal information forwarded to all distributed perimeter controllers by a high level coordinator controller.

1. Introduction

Adopting the concept of Macroscopic Fundamental Diagrams to model and control traffic flow on large-scale urban road networks have been investigated extensively during the last years, e.g. Daganzo (2007), Geroliminis and Daganzo (2008), Geroliminis et al. (2013), Haddad and Geroliminis (2012). Macroscopic Fundamental Diagrams (MFDs) provide aggregate relationships between traffic variables at urban networks, i.e. the MFD can respectively link between network vehicle density (veh/km) or accumulation (veh) and network space-mean flow or trip completion flow (veh/hr). The MFD aims at reducing the modeling complexity of the traffic flow dynamics for large-scale urban networks to develop aggregate MFD-based models. Such models are crucial in order to approach large-scale traffic control problems with model-based control methods.

* Corresponding author at: Technion City, Rabin Building, Room 726, Israel.
E-mail address: jh@technion.ac.il (J. Haddad).

http://dx.doi.org/10.1016/j.trc.2016.12.002
0968-090X/

Modeling of transportation networks based on MFDs was initially proposed by Godfrey (1969), although their theoretical foundations (e.g., the existence of MFDs) were provided later by Daganzo (2007). The MFDs were found to well describe the dynamics of a congested urban network first in Yokohama by Geroliminis and Daganzo (2008), and investigated using empirical or simulated data by Buisson and Ladier (2009), Ji et al. (2010), Mazloumian et al. (2010), Daganzo et al. (2011), Gayah and Daganzo (2011a), Zhang et al. (2013), Mahmassani et al. (1987), Olszewski et al. (1995) and others. Homogeneous (i.e., small variance of link densities) large networks have a well-defined MFD (as observed in Yokohama), i.e. low scatter of flows for the same densities (or accumulations) (Geroliminis and Sun, 2011b; Mazloumian et al., 2010; Daganzo et al., 2011; Knoop et al., 2013; Mahmassani et al., 2013). The observability of the MFD with different sensing techniques has been studied in Keyvan-Ekbatani et al. (2013), Leclercq et al. (2014), Ortigosa et al. (2014).

MFDs have been showed to enable the design of elegant control strategies to improve mobility and decrease delays in large road networks (Daganzo, 2007; Haddad and Geroliminis, 2012; Geroliminis et al., 2013; Hajiahmadi et al., 2015; Haddad et al., 2013; Aboudolas and Geroliminis, 2013; Keyvan-Ekbatani et al., 2012; Knoop et al., 2012; Zhang et al., 2013). The concept of MFDs has also been the basis of *perimeter control* strategies. In perimeter control, the idea is to manipulate the transfer flows along the perimeter of an urban region. MFD-based perimeter control has been proposed for single-region cities in Daganzo (2007), Keyvan-Ekbatani et al. (2012), Haddad and Shraiber (2014), and for multi-region cities in Haddad and Geroliminis (2012), Geroliminis et al. (2013), Aboudolas and Geroliminis (2013), Hajiahmadi et al. (2015), Haddad et al. (2013). Different control approaches have been used to solve the perimeter control problems, e.g., the Model Predictive Control approach has been used in Geroliminis et al. (2013), Haddad et al. (2013), Hajiahmadi et al. (2015), and the classical feedback control approach has been implemented in Keyvan-Ekbatani et al. (2012), Aboudolas and Geroliminis (2013), where a Proportional-Integral (PI) perimeter controller has been designed for an urban region in Keyvan-Ekbatani et al. (2012), while in Aboudolas and Geroliminis (2013) a multivariable feedback regulator for multiple regions has been designed. Recently, another type of controllers, i.e. the switching signal timing plans controller, together with the perimeter controllers, has been introduced to manage and control a large-scale urban network in Hajiahmadi et al. (2015). Moreover, route guidance strategies with the utilization of MFD have been studied in Knoop et al. (2012), Gayah and Daganzo (2011b), Yildirimoglu et al. (2015), Yildirimoglu and Geroliminis (2014), while in Xiong et al. (2016) modeling agents' en-route diversion behavior under information provision has been introduced, where the dynamic behavioral responses and network performance are represented by MFDs. In Zhang et al. (2015) integrating a Cell Transmission Model with the MFD for urban networks is proposed, while the relations between route patterns within a network and the related aggregate traffic dynamics is investigated in Leclercq et al. (2015). Recently, control design for perimeter and gating control in presence of time-delay in urban road network have been developed in Haddad and Mirkin (2016), Keyvan-Ekbatani et al. (2015), Mirkin et al. (2016). Simulation results in Xue et al. (2016) have revealed that the designed control and the resulted control performance highly depend on the system modeling.

The hysteresis phenomena and heterogeneity of urban regions challenge the dynamic modeling task based on MFD (Daganzo et al., 2011; Buisson and Ladier, 2009; Saberi and Mahmassani, 2012; Geroliminis and Sun, 2011a). The heterogeneous networks might not have a well-defined MFD, especially in the decreasing part. Partitioning such a network into homogenous regions can result in well-defined shape MFD with low scatter, as shown in Ji and Geroliminis (2012). However, if the network is *dynamically* partitioned in time and space corresponding to the congestion evolution and propagation, see Ji et al. (2014), then the shape of MFD can be expected but not explicitly determined as it might vary with time within upper and lower bound envelopes. Therefore, in order to deal with scattered MFD (not well-defined) in case of heterogeneity, and/or well-defined shape of MFD but not defined explicitly in advance in case of partitioning, one can integrate parameter uncertainties in the model to cope with such difficulties. Notably, in previous works (Geroliminis et al., 2013; Hajiahmadi et al., 2015; Haddad et al., 2013; Ramezani et al., 2015) the developed MPC solution approach for the different models has performed well for different levels of errors in the MFD's shape, given that the prediction dynamic models are sufficiently accurate. Recently in Haddad and Shraiber (2014), Haddad (2015), robust perimeter controllers have been designed to systematically take into account uncertainties in MFD-based dynamics. In Haddad and Shraiber (2014), considering a one region control problem, a robust fixed structure perimeter controller was designed with the help of quantitative feedback theory, based on a partially uncertain (interval) MFD. Haddad (2015) considers modeling and control of uncertain MFD systems for multiple-region networks. The uncertain model is utilized to design a robust feedback controller by a novel approach called Interpolation Control.

There are only few works (Aboudolas and Geroliminis, 2013; Geroliminis et al., 2013; Hajiahmadi et al., 2015; Haddad, 2015; Ramezani et al., 2015) that deal with perimeter control for *multi-region* system with MFD-based modeling, i.e. multiple regions system consisting number of homogenous regions. However, (i) none of these works deals with parameter uncertainties in the model, except Haddad (2015), and (ii) the control strategies in all these works are *centralized* oriented. E.g., the centralized optimal control design for multi-input multi-output (MIMO) problem is considered in Aboudolas and Geroliminis (2013), where the linear system model matrices are known, i.e. a nominal system model *without any uncertainties* is studied. The control objective is to stabilize the accumulation state vector around a given constant vector of accumulation reference. The proposed controller is a linear-quadratic state feedback controller (LQR), and two LQR versions of an optimization problem, without and with integral action, are studied. The LQ gain matrices are designed by linearizing the nominal nonlinear traffic dynamics around the equilibrium points. Note that unfortunately such nominal-optimal control laws do no guarantee the robustness properties with respect to uncertainties. Moreover, centralized control of an urban network even with MFD-based macroscopic approach might be still computationally complex, if many regions is considered,

which might make its implementation in real-time infeasible. To cope with computational complexity, a mixed integer linear programming problem is obtained in Hajiahmadi et al. (2015) after approximation of the nonlinear model using some techniques along with the piecewise affine approximation. The results of the case studies show the importance of the approximated model regarding the required computation time.

Although integrating multiple regions through an effective centralized control structure could enhance the large-scale network performances during heavy congestion conditions, lack of coordination among the regions' network jurisdictions and/or limited means of traffic data communication might impede such multi-region traffic network ideal goal. Hence, distributed adaptive perimeter (DAP) control schemes can be developed as potential solution for overcoming such deficiency, see Fig. 1.

An increasing number of control problems for composite interconnected systems require the use of a control structure with physically distributed controllers. Distributed control is an approach suitable to use for a wide range of large and complex systems including networked satellite control, air traffic control, and traffic flow control. There are several distributed control schemes in the literature which were introduced to other traffic control problems, e.g. the interesting idea of P0 control is suggested in Smith (1980), Smith and Mounce (2011), and max pressure is suggested in Kouvelas et al. (2014), Varaiya (2013). But these schemes consider (i) control problems at the level of signalized intersections, and in general (ii) without uncertainties in the plant model. Note that during oversaturated conditions these local distributed signal controllers might perform poorly as they are unable to integrate fast propagation of congestion and spill back effects, see e.g. the discussion in Varaiya (2013) for max pressure controllers. A suitable distributed control scheme for large-scale traffic networks is shown in Fig. 1, where there exists a large-scale traffic management center that coordinates between distributed traffic control centers, which manage and control their own urban regions. With the rapid advances in traffic detectors and sensors, e.g. probe vehicles, Bluetooth sensors, we are able to deploy systems with cheap distributed sensors, rendering local sensing.

Distributed control schemes present practical and efficient means for designing control algorithms which are based only on local information while computer networks provide an infrastructure for their realization, see e.g. the recent books (Kumar et al., 2005; Tarbouriech et al., 2005). Adaptation may also be required in order to compensate for uncertainties in the system dynamics. Distributed structures offer many well-known potential advantages with respect to centralized ones (Šiljak, 1991). On the other hand, information constraints and the always present uncertainty introduce challenging issues when designing adaptive control laws based on the locally available information with the aim to achieve a common objective.

The goal of the present paper is to take a first step towards coordinated distributed adaptive perimeter (DAP) control with state feedback for uncertain large-scale urban road networks. The urban control problems are inherently distributed in

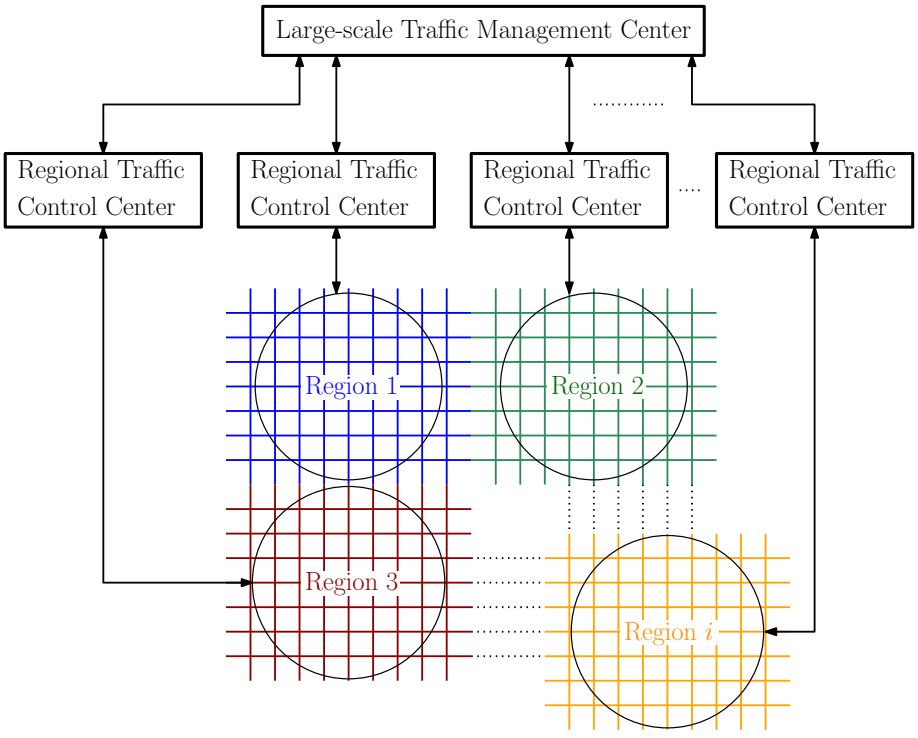

Fig. 1. Distributed adaptive perimeter (DAP) control scheme: a large-scale traffic management center that coordinates between traffic control centers for urban regions.

nature and they are typical examples of complex interconnected systems with large uncertainties. The control of such processes involves the measurement and manipulation of a large number of variables, and the ensuing complexity often makes the implementation of a centralized control strategy impossible. Hence, decentralized control, a control law based only on local information, is often preferable. A common approach to distributed control design is to impose information constraints on the controller structure. Such constraints, however, may greatly complicate the control design procedure.

The problem of urban traffic perimeter control in this work is a control problem with a distributed control structure. Such structure is a consequence of the constraints that are imposed on the information flow within the system. In such a structure the perimeter controllers operate completely independently from each other, i.e. each local perimeter controller may on-line measure only a subset the variables of the network. The coordinated distributed control structure, shown in Fig. 3, is used for the control design, where an upper control level (coordinator or the large-scale traffic management center) coordinates the functioning of the local perimeter controllers by providing also the reference signals of the other urban regions, so called model co-ordination. To design the perimeter control law, we utilize the control oriented MFD model presented in Haddad and Mirkin (2016) in its *interconnected form*, and take into account uncertainty of model parameters and unknown bounded external disturbances.

2. Control oriented dynamic model of urban traffic networks

A new control oriented dynamic model for R interconnected regions is presented. The presented model is based on the model introduced for the coupled control scheme in Haddad and Mirkin (2016). In this paper, the model is developed for a more general control case - the uncoupling control scheme.

2.1. Basic nonlinear model design

Let us consider a large-scale urban network decomposed into R homogeneous urban subnetworks (regions), each having a partial uncertainty MFD, as shown in Fig. 2.

Let us denote $d_{ij}(t)$ (veh/s) as the traffic flow demand generated in region i with direct destination to region j. Here $i = 1, \ldots, R$ and $j \in S_i$, where S_i defines the set of the regions, with which the region i can communicate, i.e. the set of regions that are directly reachable from region i. Each of S_i is a set of integers corresponding to the region's index number. The dynamical model of the each interacting with other urban region i, $i = 1, \ldots, R$ is derived in several steps. Corresponding to the traffic demands, the dynamical system states (accumulations) are defined as: $n_{ii}(t)$ (veh) is the total number of vehicles in region i with destination to inside the region; $n_{ij}(t)$ (veh) is the total number of vehicles in region i with direct destination to region j; and $n_i(t)$ (veh) is the accumulation or the total number of vehicles in region i, that is

$$n_i(t) = n_{ii}(t) + \sum_{j \in S_i} n_{ij}(t). \tag{1}$$

The mass conservation equations of the R-region system are as follows, based on Haddad and Mirkin (2016),

$$\begin{aligned} \dot{n}_{ii}(t) &= -q_{ii}^{\text{ins}}(t) + \sum_{j \in S_i} q_{ji}^{\text{in}}(t) + d_{ii}(t) \\ \dot{n}_{ij}(t) &= -q_{ij}^{out}(t) + d_{ij}(t) \\ n_i(t) &= n_{ii}(t) + \sum_{j \in S_i} n_{ij}(t) \end{aligned} \tag{2}$$

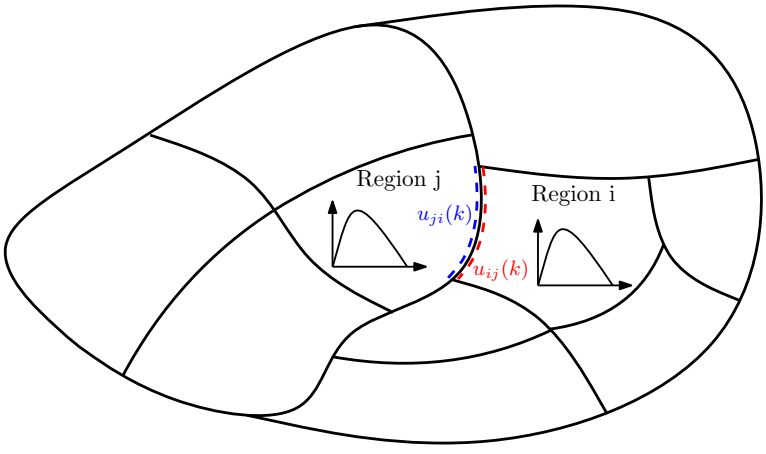

Fig. 2. A schematic large-scale urban network decomposed into R regions.

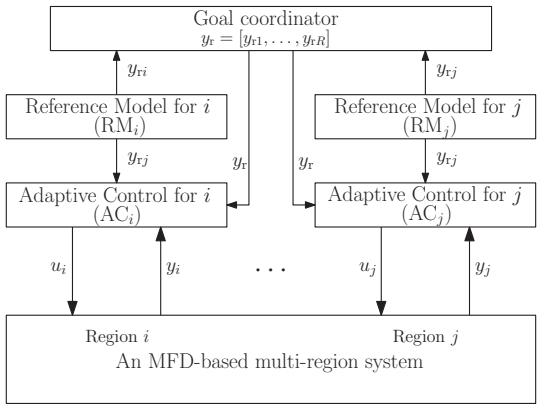

Fig. 3. A distributed adaptive perimeter (DAP) control structure with coordination.

where the variables $q_{ji}^{\text{in}}(t)$ (veh/s) and $q_{ij}^{\text{out}}(t)$ (veh/s) denote the input and output transfer flows with the corresponding direction (from region j to i or from region i to j). The variable $q_{ii}^{\text{ins}}(t)$ (veh/s) is the internal traffic flow, i.e. trips of region i with internal destination (inside the region). Note that in this paper the boundary capacities between regions are ignored. The boundary capacity constraints can be imposed on the R-region system similarly to Eq. (4) in Ramezani et al. (2015). However, it should be stressed that the boundary capacity constraints can be ignored as they will not be active constraints. The boundary capacity depends on the accumulation as a piecewise linear function, i.e. it is approximated as a constant high value, which is larger than the corresponding transfer flow, for a range of accumulations, and it starts to decrease at an accumulation which is much larger than the critical accumulation. The controllers aim to operate the dynamic system close to the critical accumulations and far from the maximum accumulations (gridlock), therefore, the boundary capacity constraints can be ignored. It should be also noted that recently an MFD-based model for two-region networks with aggregate boundary queue dynamics was introduced in Haddad (2017).

2.2. Nonlinear R-region model in interconnected form

In the following, we write the dynamic model of R regions (2) as a dynamic system consists of R subsystems that are interconnected.

To derive control oriented traffic flow dynamic model in *interconnected form*, we first rewrite (2) as

$$\begin{aligned}
&\begin{bmatrix} \frac{dn_{ii}(t)}{dt} \\ \frac{dN_i(t)}{dt} \end{bmatrix} = \begin{bmatrix} \sum_{j\in S_i} q_{ji}^{\text{in}}(t) - q_{ii}^{\text{ins}}(t) \\ -Q_i(t) \end{bmatrix} + \begin{bmatrix} d_{ii}(t) \\ d_i(t) \end{bmatrix} \\
&n_i(t) = n_{ii}(t) + \sum_{j\in S_i} n_{ij}(t), \quad i = 1, \ldots, R
\end{aligned} \tag{3}$$

where

$$\begin{aligned}
&N_i(t) = \mathbf{Vec}_{j\in S_i} n_{ij}(t) \in \mathbb{R}^{card(S_i)}, \quad Q_i(t) = \mathbf{Vec}_{j\in S_i} q_{ij}^{\text{out}}(t) \in \mathbb{R}^{card(S_i)} \\
&d_i(t) = \mathbf{Vec}_{j\in S_i} d_{ij}(t) \in \mathbb{R}^{card(S_i)},
\end{aligned} \tag{4}$$

and $\mathbf{Vec}_{j=1}^{m} z_j = [z_1, \ldots, z_m]^{\text{T}}$ is the vectorization notation. The vector $z(t) = \mathbf{Vec}_{j\in S_i} z_j$ has the dimension $card(S_i)$, i.e. $z(t) \in \mathbb{R}^{card(S_i)}$ and the symbol $\mathbf{card}(S_i)$ denotes the cardinality (size) of S_i. Based on the macroscopic fundamental diagram (MFD) concept, the internal, input and output traffic flows of region i can be calculated corresponding to some relationships between accumulations, see Haddad and Mirkin (2016), Geroliminis et al. (2013), namely in the form of the following weighted nonlinear relations,

$$q_{ii}^{\text{ins}}(t) = M_{ii}(n_{ii}(t), n_i(t)) = \frac{n_{ii}(t)}{n_i(t)} G_i(n_i(t)) - [\text{flow with internal direction}], \tag{5}$$

$$\begin{aligned}
&q_{ij}^{\text{out}}(t) = M_{ij}(n_{ij}(t), n_i(t)) = \frac{n_{ij}(t)}{n_i(t)} G_i(n_i(t)) - [\text{flow with direction from } i \text{ to } j,\ j \in S_i], \\
&q_{ji}^{\text{in}}(t) = M_{ji}(n_{ji}(t), n_j(t)) = \frac{n_{ji}(t)}{n_j(t)} G_j(n_j(t)) - [\text{flow with direction from } j \text{ to } i,\ i \in S_j],
\end{aligned}$$

where $G_i(n_i(t))$ (veh/s) denotes the appropriate MFD parametrization for region i, i.e. the nonlinear relationship between the trip completion flow G_i and the accumulation $n_i(t)$ (veh).

To be able to regulate the input $q_{ji}^{\text{in}}(t)$ and output $q_{ij}^{\text{out}}(t)$ flows at the perimeter border of region i, we define the input and output flows as adjustable controlled flows in the following form:

$$\begin{aligned} q_{ij}^{\text{out}}(t) &= M_{ij}(n_{ij}(t), n_i(t))u_{ij}(t) - [\text{controlled flow from } i \text{ to } j,\ j \in S_i], \\ q_{ji}^{\text{in}}(t) &= M_{ji}(n_{ji}(t), n_j(t))u_{ji}(t) - [\text{controlled flow from } j \text{ to } i,\ i \in S_j], \end{aligned} \tag{6}$$

where the variables $u_{ji}(t)$ and $u_{ij}(t)$ represent the perimeter control inputs, which are introduced on the border between the regions i and j, to control the transfer flows between the regions.

Now we introduce for i-th local region the following state $X_i(t), U_i$ and disturbance $D_i(t)$ vectors:

$$\begin{aligned} X_i(t) &= [n_{ii}(t),\ N_i^{\text{T}}(t)]^{\text{T}} \in \mathbb{R}^{\text{card}(S_i)+1}, \\ U_i(t) &= \mathbf{Vec}_{j\in S_i} u_{ij}(t) \in \mathbb{R}^{\text{card}(S_i)}, \\ D_i(t) &= [d_{ii}(t),\ d_i^{\text{T}}(t)]^{\text{T}} \in \mathbb{R}^{\text{card}(S_i)+1}, \end{aligned} \tag{7}$$

and define the nonlinear vector functions $F_i(n_{ii}, n_i) \in \mathbb{R}^{1+card(S_i)}$ and $F_{ji}(n_{ji}, n_j) \in \mathbb{R}^{1+card(S_i)}$

$$-F_i(n_{ii}, n_i) = \begin{bmatrix} M_{ii}(n_{ii}, n_i)_{1\times 1} \\ 0_{card(S_i)\times 1} \end{bmatrix}, \quad F_{ji}(n_{ji}, n_j) = \begin{bmatrix} M_{ji}(n_{ji}(t), n_j(t))_{1\times 1} \\ 0_{card(S_i)\times 1} \end{bmatrix}. \tag{8}$$

Then, in view of (4)–(8), from (3) one obtains the following general nonlinear dynamical model in interconnected form for R-region systems operating in the nominal mode (i.e., model that is designed for the nominal MFD):

$$\begin{aligned} \dot{X}_i(t) &= F_i(n_{ii}(t), n_i(t)) + B_i\big(n_1(t), \ldots, n_{\text{card}(S_i)}(t)\big)U_i(t) + D_i(t) + \sum_{j\in S_i} F_{ji}\big(n_{ji}(t), n_j(t)\big)u_{ji}(t) \\ n_i(t) &= n_{ii}(t) + \sum_{j\in S_i} n_{ij}(t) \\ Y_i(t) &= n_i(t) = C_i^T X_i(t), \quad C_i^T = \underbrace{[1, \ldots, 1]}_{\text{card}(S_i)+1}, \quad i = 1, \ldots, R, \end{aligned} \tag{9}$$

where for $i = 1, \ldots, R$; $j \in S_i$

$$\begin{aligned} B_i\big(n_1(t), \ldots, n_{\text{card}(S_i)}(t)\big) &= \begin{bmatrix} 0_{1\times card(S_i)} \\ B_{di} \end{bmatrix} \in \mathbb{R}^{(1+\text{card}(S_i))\times \text{card}(S_i)}, \\ B_{di}\big(n_1(t), \ldots, n_{\text{card}(S_i)}(t)\big) &= \mathbf{Dg}_{j\in S_i} M_{ij}(n_{ij}(t), n_i(t)) \in \mathbb{R}^{\text{card}(S_i)\times \text{card}(S_i)}, \end{aligned} \tag{10}$$

and the symbol $\mathbf{Dg}_{j=1}^{m} z_j = diag\{z_1, \ldots, z_m\}$.

2.3. Linearized model for DAP control design

To deal with the uncertainties in the traffic dynamics of the nonlinear model (9), in this work, we will employ a linearization-based distributed adaptive control design. We linearize the nonlinear model (9) at multiple operating points $\left(X_o^k, U_o^k\right), k = 1, \ldots, \kappa$, where κ denotes the number of operating scenarios. The operating points may not be equilibrium points due to system uncertainties. The operating points are selected to represent the various urban regions functioning conditions.

Then, the uncertain state space model, which are composed of R multi-input ($u_i(t)$) single-output ($y_i(t)$) interconnected regions with set of unknown parameters, corresponding to different points of linearization and suitably initialized, can be used to characterize the linearized system with uncertainties:

$$\begin{aligned} \dot{x}_i(t) &= A_i^k x_i(t) + B_i^k u_i(t) + B_i^k d_i(t) + \sum_{j\in S_i} A_{ij}^k x_j(t) + \sum_{j\in S_i} p_{ji}^k(x_j(t)), \\ y_i(t) &= n_i(t) = c_i^T x_i(t), \quad c_i^T = \underbrace{[1, \ldots, 1]}_{\text{card}(S_i)+1},\ i = 1, \ldots, R, \end{aligned} \tag{11}$$

where $x_i(t) = X_i(t) - X^k{}_{io} \in \mathbb{R}^{card(S_i)+1}, u_i(t) = U_i(t) - U^k{}_{io} \in \mathbb{R}^{card(S_i)}, d_i(t) = D_i(t) - D_{io} \in \mathbb{R}^{card(S_i)}$ and $y_i(t) \in \mathbb{R}$ are the state, input, disturbance and output of the i-th region, respectively. The constant system parameter matrices $A_i^k \in \mathbb{R}^{(1+card(S_i))\times(card(S_i)+1)}, B_i^k \in \mathbb{R}^{(1+card(S_i))\times card(S_i)}$, $A_{ij}^k \in \mathbb{R}^{(1+card(S_i))\times(card(S_j)+1)}$ are being *unknown*. The nonlinear term $\sum_{j\in S_i} p_{ij}(x_j(t))$ represents the linearization uncertainties, namely: the higher-order terms after linearization (residual approximation errors inherent in the linear parameterization of the system uncertainty) and an unknown dynamics offset (introduced by the

non-equilibrium operating points). Keeping in mind that the relationships, that describe the MFD are *always bounded functions*, see e.g. Haddad and Shraiber (2014), Laval and Castrillón (2015), Haddad (2015), we will consider nonlinear perturbations $p_{ij}(x_j(t))$ as a bounded by some unknown constants and to reflect the MFD partial uncertainty, we will consider these constants as *unknown*.

The system dynamics are therefore given by (11) are used for distributed adaptive control design. For control synthesis it is assumed that:

- the parameters matrices of (11) are *unknown* due to varying external conditions (plant with parametric uncertainties), and
- there are external bounded disturbances (demands) and nonlinear perturbations with *unknown* bounds.

An adaptive control, to accommodate the parametric uncertainties and compensate for the unknown disturbances, is therefore should be considered for control of this system.

3. Distributed adaptive perimeter control design

3.1. The control structure and objective

A distributed adaptive control structure with coordination is proposed, as shown in Fig. 3. The system consists of a plant, a set of adaptive controllers $(\mathrm{AC}_i, \ldots, \mathrm{AC}_j)$ and the corresponding reference models $(\mathrm{RM}_i, \ldots, \mathrm{RM}_j)$.

Our control objective is to construct distributed local state feedback control laws $u_i(t)$ in (11) to make all the closed-loop signals bounded, and the output signals $y_i(t)$ asymptotically track given reference signals $y_{ri}(t) \in \mathbb{R}$ from R stable local reference models

$$\begin{aligned} &\dot{x}_{ri}(t) = A_{ri}x_{ri}(t) + B_{ri}r_i(t), \\ &y_{ri}(t) = c_i x_{ri}(t), \quad c_i = [1, \ldots, 1]^T, \quad i = 1, \ldots, R, \end{aligned} \tag{12}$$

where for the i-th model, $x_{ri}(t)$ is the state vector postulated to belong to $\mathbb{R}^{card(S_i)+1}$ and $r_i(t) \in \mathbb{R}^{card(S_i)}$ is an appropriate reference input allowing the region output $y_i(t)$ to be equal to the desired signal $y_{ri}(t)$. The matrices A_{ri} and B_{ri} are known constant matrices of appropriate dimensions.

3.2. Proposed distributed adaptive controller structure

The distributed adaptive control scheme with *reference model coordination*, refer to e.g. Mirkin (2003), Mirkin and Gutman (2003), Mirkin et al. (2012), is used to achieve the control objective. The control law for the i-th region $u_i(t)$ is chosen to be of the form

$$u_i(t) = u_{li}(t) + u_{ci}(t), \quad i = 1, \ldots, R, \tag{13}$$

where the component $u_{li}(t)$ is based only on *local* signals of the i-th region, and $u_{ci}(t)$ is the *coordinated* component which is based on the reference signals of all other regions. In the following, suitable parameterizations of the local and coordinated components of the control law (13) are chosen to anticipate the uncertainty effects.

3.2.1. Control component based only on local information

The part of the control law, $u_{li}(t)$, which is based only on the local information is parameterized as follows

$$\begin{aligned} &u_{li}(t) = \theta_i^T(t)e_i(t) + u_{lik}(t), \quad e_i(t) = x_i(t) - x_{ri}(t), \\ &u_{lik}(t) = -\sum_{k=1}^{card(S_i)} \gamma_{ik} \int_0^t E_{ik}(t)\mathrm{d}t, \end{aligned} \tag{14}$$

where $\theta_i(t) \in \mathbb{R}^{(1+card(S_i))\times card(S_i)}$ is the adaptation gain matrix, and the constant scalars $\gamma_{ik} > 0$ are some design parameters. $E_{ik}(t) \in \mathbb{R}$ is the k-th element of the vector $e_i^T(t)P_iB_{ri}$ $(k = 1, \ldots, card(S_i))$ and the matrix $P_i = P_i^T > 0$ is the solution of the following Lyapunov equation

$$A_i^T P_i + P_i A_i + Q_i = 0, \quad Q_i = Q_i^T > 0. \tag{15}$$

3.2.2. Coordinated control component

The coordinated control component, $u_{ci}(t)$, which is based on the reference signals of all other regions is chosen as follows

$$u_{ci}(t) = \sum_{j \in S_i} \theta_{ij}^T(t)x_{rj}(t), \tag{16}$$

where $\theta_{ij}(t) \in \mathbb{R}^{(1+card(S_j))\times card(S_i)}$ is the adaptation gain matrix.

3.2.3. Adaptation algorithms

The adaptation algorithms are chosen as follows, $i = 1, \ldots, R$ and $j \in S_i$,

$$\begin{aligned}
&\theta_i(t) = -\eta_i(0) - \eta_i(t) - \eta_i(t-h_i) - \int_0^t \eta_i(s)\mathrm{d}s,\\
&\eta_i^T(t) = \gamma_i S_{pi} e_i^T(t) P_i B_{ri} e_i^T(t),\\
&\theta_{ij}(t) = -\eta_{ij}(0) - \eta_{ij}(t) - \eta_{ij}(t-h_{ij}) - \int_0^t \eta_{ij}(s)\mathrm{d}s,\\
&\eta_{ij}^T(t) = \gamma_{ij} S_{pi} e_i^T(t) P_i B_{ri} x_j^T(t),
\end{aligned} \tag{17}$$

or in differential forms

$$\begin{aligned}
&\dot{\theta}_i(t) = -\eta_i(t) - \dot{\eta}_i(t) - \dot{\eta}_i(t-h_i),\\
&\eta_i^T(t) = \gamma_i S_{pi} e_i^T(t) P_i B_{ri} e_i^T(t),
\end{aligned} \tag{18}$$

$$\begin{aligned}
&\dot{\theta}_{ij}(t) = -\eta_{ij}(t) - \dot{\eta}_{ij}(t) - \dot{\eta}_{ij}(t-h_{ij}),\\
&\eta_{ij}^T(t) = \gamma_{ij} S_{pi} e_i^T(t) P_i B_{ri} x_j^T(t),
\end{aligned} \tag{19}$$

where the gains γ_i and γ_{ij} and the scalars $h_i > 0$ and $h_{ij} > 0$ are some design parameters.

Remark 1. Although only the integral component $\eta_i(t)$ ($\dot{\eta}_i(t) = 0$ and $\dot{\eta}_i(t-h_i) = 0$ in (18)) of the adaptation algorithm is needed for stability and exact asymptotic tracking, the use of the proportional $\dot{\eta}_i(t)$ and the proportional delayed $\dot{\eta}_i(t-h_i)$ terms in the adaptation algorithm (18) makes it possible to achieve better adaptation performance than the traditional I and PI schemes, refer to Mirkin and Gutman (2010).

3.3. Main result

The following theorem gives the main result.

Theorem 1. *Consider the uncertain system in (11) and the reference models in (12). Then, the adaptive perimeter control (13)–(16) with adaptation rules (17) assure that (i) the closed-loop signals are bounded, and (ii) all tracking errors $e_i(t), i = 1, \ldots, R$, converge to zero asymptotically. Therefore, the local outputs $y_i(t)$ asymptotically track the reference model outputs $y_{ri}(t)$. The reference model dynamics can be chosen such that the local outputs $y_i(t)$ track specified external signals e.g. constants.*

Proof 1. See Appendix A.

4. Numerical study: distributed adaptive perimeter control for interconnected two and three urban regions

In this section, we demonstrate the possibilities of the developed adaptive control scheme by studying the problem of DAP control for an urban traffic network, composed of two or three regions under incompletely specified plant models.

4.1. Two urban regions model

Following the general model for R regions presented in (11), one gets the following system model for the case of two regions

$$\begin{aligned}
&n_1(t) = n_{11}(t) + n_{12}(t); card(S_1) = card(S_2) = 1; N_1(t) = n_{12}(t);\\
&N_2(t) = n_{21}(t); B_{d1} = M_{12}(n_{12}(t), n_1(t)); \quad B_{d2} = M_{21}(n_{21}(t), n_2(t)).
\end{aligned} \tag{20}$$

Using (20) and in view of (11), the uncertain linearized traffic model with parametric uncertainties and external bounded disturbances with unknown bounds can be written as

$$\begin{aligned}
&\dot{x}_1(t) = A_1 x_1(t) + b_1 u_1(t) + A_{12} x_2(t) + b_1(d_1(t) + p_{12}(x_1, x_2)),\\
&n_1(t) = c_1^T x_1(t),\\
&\dot{x}_2(t) = A_2 x_2(t) + b_2 u_2(t) + A_{21} x_1(t) + b_2(d_2(t) + p_{21}(x_1, x_2)),\\
&n_2(t) = c_2^T x_2(t),
\end{aligned} \tag{21}$$

where

$$x_1(t) = \begin{bmatrix} n_{11}(t) \\ n_{12}(t) \end{bmatrix} = \begin{bmatrix} \text{the number of vehicles in region 1 with destination inside the region} \\ \text{the number of vehicles in region 1 with destination to region 2} \end{bmatrix},$$

$$x_2(t) = \begin{bmatrix} n_{22}(t) \\ n_{21}(t) \end{bmatrix} = \begin{bmatrix} \text{the number of vehicles in region 2 with destination inside the region} \\ \text{the number of vehicles in region 2 with destination to region 1} \end{bmatrix},$$

the outputs $n_i(t) = [\text{vehicles' number in the region}]$ $(i = 1, 2)$ and the perimeter controllers for regions $1, 2$ are $u_1(t), u_2(t) \in \mathbb{R}$, respectively. This means that for this simulation example, we deal with an urban network decomposed into two urban regions, where each region model is described by a two-dimensional state vector, a scalar perimeter control input, and a scalar output.

Remark 2. It is important to note that in the linearized system model (21), the partially unknown forms of MFDs (uncertainties) are placed within the adaptive control design as *unknown* constant parameter matrices $A_1, b_1, A_{12}, c_1, A_2, b_2, A_{21}, c_2$, the bounded by *unknown* values disturbances $d_1(t), d_2(t)$ (which are the traffic flow demands) and the unknown nonlinear perturbations $p_{12}(x_1, x_2), p_{21}(x_1, x_2)$, which include also the linearization (approximation errors). Specificity of the MFD shape allows us to consider it in this study as a bounded by some *unknown* constants p_{o1}, p_{o2}, i.e. $|p_{12}(x_1, x_2)| < p_{o1}, |p_{21}(x_1, x_2)| < p_{o2}$. Instead, in the presented numerical study these boundaries are included into the uncertain $d_i(t)$. The only information available to the controller is the structural information given in Assumptions (A1)-(A4).

Remark 3. Note also that the set of approximated MFD functions will result after linearization the same unified model matrices structure, but with different values of its parameters. Using varying operating points are also incorporated in the linearized dynamics, as different values of the model parameters under the same unified structure.

4.2. Three urban regions model

For the case of three regions we investigated the following system structure

$$\begin{aligned}
&\dot{x}_1(t) = A_1 x_1(t) + b_1 u_1(t) + A_{13} x_3(t) + b_1 d_1(t), \\
&n_1(t) = c_1^T x_1(t), \quad x_1(t) = [n_{11}(t)\ n_{13}(t)]^T \in \mathbb{R}^2 \\
&\dot{x}_2(t) = A_2 x_2(t) + b_2 u_2(t) + A_{23} x_3(t) + b_2 d_2(t), \\
&n_2(t) = c_2^T x_2(t), \quad x_2(t) = [n_{22}(t)\ n_{23}(t)]^T \in \mathbb{R}^2 \\
&\dot{x}_3(t) = A_3 x_3(t) + b_3 u_3(t) + A_{31} x_1(t) + A_{32} x_2(t) + b_3 d_3(t) \\
&n_3(t) = c_3^T x_3(t), \quad x_3(t) = [n_{33}(t)\ n_{31}(t)\ n_{32}(t)]^T \in \mathbb{R}^3
\end{aligned} \tag{22}$$

Remark 4. It is important to note a specific feature of the control problem, that if an urban region is interconnected with more than one region, the dimension of its states is different, e.g. $x_1(t), x_2(t) \in \mathbb{R}^2$, and $x_3(t) \in \mathbb{R}^3$ in (22).

4.3. Control goals formalization

In this simulation, the goal of each region is to reach a desired (constant) regional accumulation n_i^*, which is determined by the coordinator, i.e. the large-scale traffic management center. Since our approach to build the adaptive distributed controller is a model reference design, we choose the reference models that capture the desired region accumulations as

$$\begin{aligned}
&\dot{x}_{r1}(t) = A_{r1} x_{r1}(t) + b_{r1} r_1(t), \quad x_{r1}(t) \in \mathbb{R}^2 \\
&n_{r1}(t) = c_1^T x_{r1}(t),\ c_1^T = [1 \quad 1], \\
&\dot{x}_{r2}(t) = A_{r2} x_{r2}(t) + b_{r2} r_2(t), \quad x_{r2}(t) \in \mathbb{R}^2, \\
&n_{r2}(t) = c_2^T x_{x2}(t),\ c_2^T = [1 \quad 1], \\
&\dot{x}_{r3}(t) = A_{r3} x_{r3}(t) + b_{r3} r_3(t), \quad x_{r3}(t) \in \mathbb{R}^3, \\
&n_{r3}(t) = c_3^T x_{x3}(t),\ c_2^T = [1 \quad 1 \quad 1].
\end{aligned} \tag{23}$$

The desired pair of matrices A_{ri}, b_{ri} in (23) are selected such that the reference model has a fast dynamics, and so it shortly provides a desired constant output $n_{ri} = n_i^*$. The objective of control is to make $n_i(t)$ tends to $n_{ri}(t) (= n_i^*)$ asymptotically, i.e. $n_i(t) \to n_i^*$ if $t \to \infty$ for $i = 1, 2, 3$.

Remark 5. It should be stressed that the main focus in this simulation study is on the regulation problem: stabilizing the regional accumulation at a given *constant steady-state* level. However, our design approach can be utlized for arbitrary time-varying desired behavior, which can be realized by tracking a *desired time function*.

4.4. Distributed adaptive perimeter controllers

The distributed adaptive perimeter controllers in our numerical study are

$$\begin{aligned} u_i(t) &= u_{Ii}(t) + u_{ci}(t), \quad i = 1,2,3; \\ u_{Ii}(t) &= \theta_i^T(t) e_i(t) - \gamma_i \int_0^t E_i(t)\mathrm{d}t, \\ u_{ci}(t) &= \theta_{ij}^T(t) x_{rj}(t),\ j \neq i. \end{aligned} \tag{24}$$

with adaptation algorithms

$$\begin{aligned} \dot{\theta}_i(t) &= -\Gamma_i \mathrm{PITD}_i(E_i(t)e_i(t)), \\ \dot{\theta}_{ij}(t) &= -\Gamma_{ij} \mathrm{PITD}_{ij}\big(E_i(t)x_{rj}(t)\big), \end{aligned} \tag{25}$$

where $\mathrm{PITD}(\bigstar)$ is the operator form for $\mathrm{PITD}_i(Z_i(t)) = k_{Ii}\int_0^t Z_i(s)ds + k_{Pi}Z_i(t) + k_{Di}Z_i(t-h_i)$ and $\mathrm{PITD}_{ij}\big(Z_{ij}(t)\big) = k_{Iij}\int_0^t Z_{ij}(s)ds + k_{Pij}Z_{ij}(t) + k_{Dij}Z_{ik}(t-h_{ij})$.

4.5. Numerical results

For a comparison study, we have tested the same adaptive controller (24) with adaptation gain rules from (25) (without retuning), for two interacting regions in Examples 1–3 and three such regions in Example 4, respectively with the same structure of reference model, to different matrices of parameters and disturbance signals of the system. Different levels of desired regional accumulations are also examined.

Based on available operating traffic conditions, models of the interconnected regions are obtained after linearization for two operating points $n_o = 0.95n_{cr}$ and $n_o = 0.8n_{cr}$ of the nominal regional MFD and 60% and 140% of its nominal values. For the nominal dynamic regional model, we use the MFD parameterization whose pattern matches the MFD observed in Yokohama, refer to Geroliminis and Daganzo (2008), denoted by $\mathrm{MFD}_{\mathrm{Yok}}$ with $n_{cr} = 3400$ (veh), $G(n_{cr}) = 6.3$ (veh/s) (see Fig. 4).

The equivalent bounded disturbances which can include both internal (e.g. off-street parking for taxis and pockets for private vehicles) and external non-controlled inflows are chosen in the following different variants (Examples 1–3): (i) $d_1(t) = 40 + 40\mathrm{Square}(0.09t)$ (rad/s), $d_2(t) = 40 + 30\mathrm{Square}(0.08t)$ (rad/s), (ii) $d_1(t) = d_2(t) = 40$, and (iii) $d_1(t) = 40 + 70\mathrm{Square}(0.1t)$ (rad/s), $d_2(t) = 40 + 60\mathrm{Square}(0.07t)$ (rad/s). Variants (i) and (iii) respectively simulate a peak hour with high and low demands with the help of "square" flow profiles, while variant (ii) simulates constant disturbance flow profile. The design parameter values for both DAP controllers in (24), (25) are listed in Table 1 (Examples 1–3).

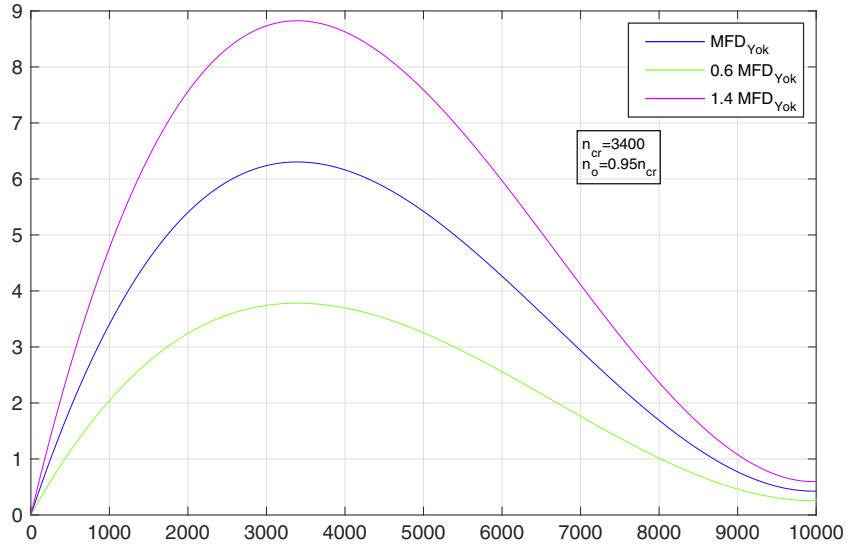

Fig. 4. Three shapes of MFD: nominal shape (blue color), 60% (green) and 140% (pink) of the nominal shape.

Table 1
Reference model dynamics and adaptive perimeter controller parameters.

Parameter	Value
$A_{r1} = A_{r2}$	$\begin{bmatrix} 0 & 1 \\ -8 & -13 \end{bmatrix}$
$b_{r1} = b_{r2}$	$[0 \quad 1]^T$
$\Gamma_1 = \Gamma_1 = \Gamma_{12} = \Gamma_{21}$	$\begin{bmatrix} 1 & 0 \\ 0 & 1 \end{bmatrix}$
$k_{P1} = k_{P2} = k_{P12} = k_{P21}$	18
$k_{I1} = k_{I2} = k_{I12} = k_{I21}$	90
$k_{D1} = k_{D2} = k_{D12} = k_{D21}$	9
$\gamma_1 = \gamma_2$	1
$Q_1 = Q_2$ from (15)	$\begin{bmatrix} 5 & 0 \\ 0 & 5 \end{bmatrix}$
$P_1 = P_2$ from (15)	$\begin{bmatrix} 5.7933 & 0.3125 \\ 0.3125 & 0.2163 \end{bmatrix}$

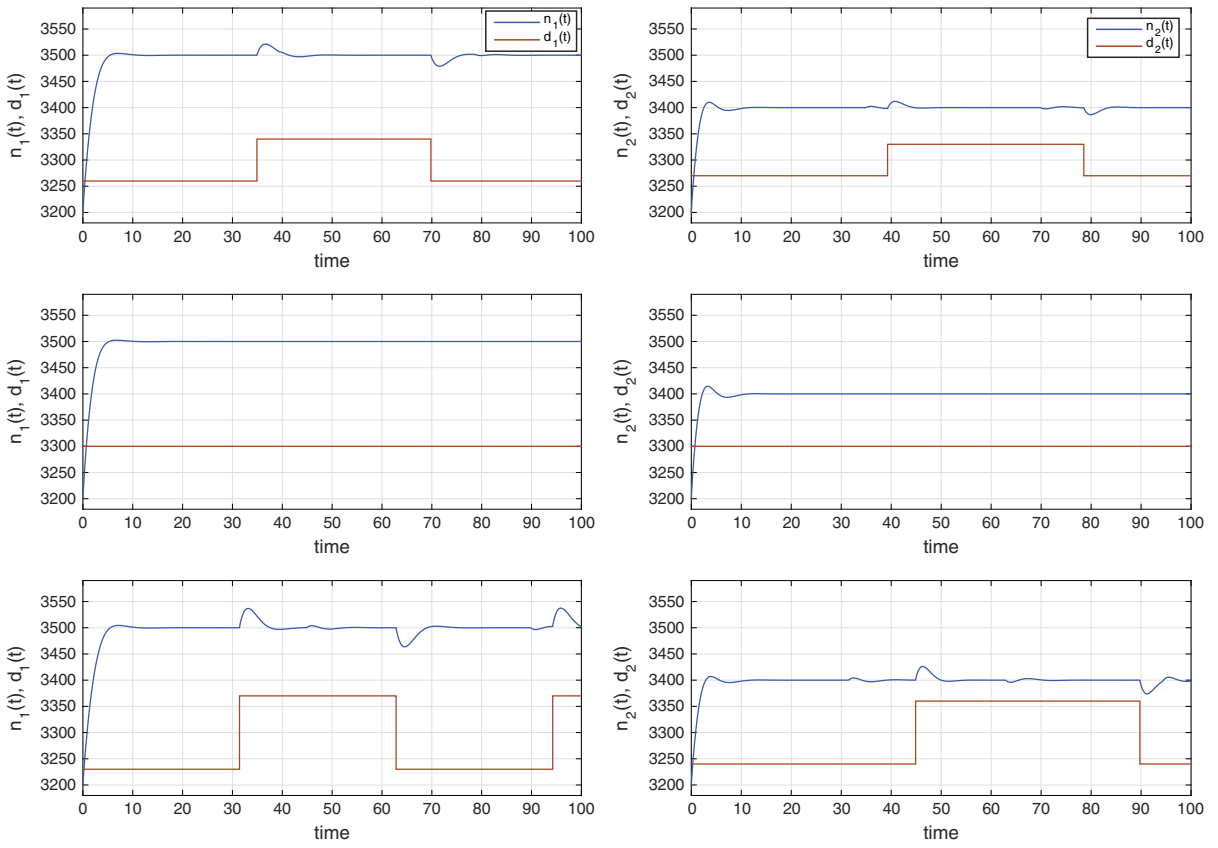

Fig. 5. Example 1a: simulation of the adaptive control system for the model (21) with the plant coefficients (26) and the controllers (24), (25) with the parameters from Table 1. The graphs show the time history of the outputs $n_1(t), n_2(t)$ and the disturbances $d_1(t), d_2(t)$ for the two regions. The left subplots are the cases of $n_1^* = 3500$ (veh) and the right subplots are the cases of $n_2^* = 3400$ (veh), $n_o = 0.95 n_{cr}$, $\mathrm{MFD}_1 = \mathrm{MFD}_2 = \mathrm{MFD}_{\mathrm{Yok}}$, $n_1(0) = n_2(0) = 3200$ (veh).

The first three numerical examples are presented for the case of two regions. In Examples 1 and 2, both regions have the same MFD and the same operating points, i.e. to which the system dynamics are linearized around. In Example 1, the adaptive perimeter controllers are examined for operating points that are close to the critical points, i.e. $n_o = 0.95 n_{cr}$, while in Example 2 the operating points are far from the critical points, i.e. $n_o = 0.8 n_{cr}$. Example 3 tests the adaptive perimeter controllers for different shapes of MFD.

Example 1. Three cases are tested in Example 1. For all cases, we consider two identical models for both regions having the same MFD shape, $\mathrm{MFD}_1 = \mathrm{MFD}_2 = \mathrm{MFD}_{\mathrm{Yok}}$. Hence, the coefficients of the plant (21) in a controllable canonical form are

$$A_1 = A_2 = \begin{bmatrix} 0 & 1 \\ -5.4683 & -12.5423 \end{bmatrix}, \quad A_{12} = A_{21} = \begin{bmatrix} 0 & 0 \\ 0.9843 & 2.2576 \end{bmatrix},$$
$$b_1 = b_2 = [0 \quad 1]^T, \quad c_1 = c_2 = [546.6614 \quad 43.5240]. \tag{26}$$

Moreover, both regions are initially uncongested with the same initial accumulations $n_1(0) = n_2(0) = 3200$ (veh). The operating points for both regions are the same, determined as $n_o = 0.95 n_{cr} = 3230$ (veh).

The simulation results of the adaptive control system for the model (21), with the plant coefficients (26), and the controllers (24), (25), with the parameters from Table 1, are shown in Figs. 5–7 for cases 1a, 1b, and 1c, respectively. The results for each case illustrate the time response of the regional model outputs, i.e. $n_1(t)$ and $n_2(t)$, for the three different variants of disturbances $d_1(t), d_2(t)$.

In cases 1a and 1b, we run the simulation for different accumulation references. The results in Fig. 5 are shown for the case 1a where the accumulation reference for region 1 is congested, i.e. $n_1^* = 3500$ (veh), and the accumulation reference for region 2 is equal to the critical accumulation $n_2^* = 3400$ (veh). While in Fig. 6, the results are shown for the reverse case, where the accumulation reference for region 1 is equal to the critical accumulation $n_1^* = 3400$ (veh), and the accumulation reference for region 2 is congested, i.e. $n_2^* = 3500$ (veh). Note that although the MFDs for both regions and the initial accumulations are the same, the reverse case is a further examination for a different combination of disturbances, since the disturbance variants are not the same for both regions.

The results of Examples 1a and 1b show that the adaptive perimeter controllers can perform well for different conditions of accumulation references, e.g. a congested accumulation reference for region 1 $n_1^* = 3500$ (veh) in Fig. 5, and for a congested accumulation reference $n_2^* = 3500$ (veh) in Fig. 6. The performance of the adaptive perimeter controllers is numerically investigated for the three variants of demand (disturbances). The results show that the adaptive perimeter controllers can reject all given variants of disturbance.

Example 1 is further utilized in case 1c to examine the designed perimeter controllers for different unequal initial accumulations $n_1(0) = 3000$ (veh) and $n_2(0) = 2900$ (veh). The results for this case are shown in Fig. 7. The results verify

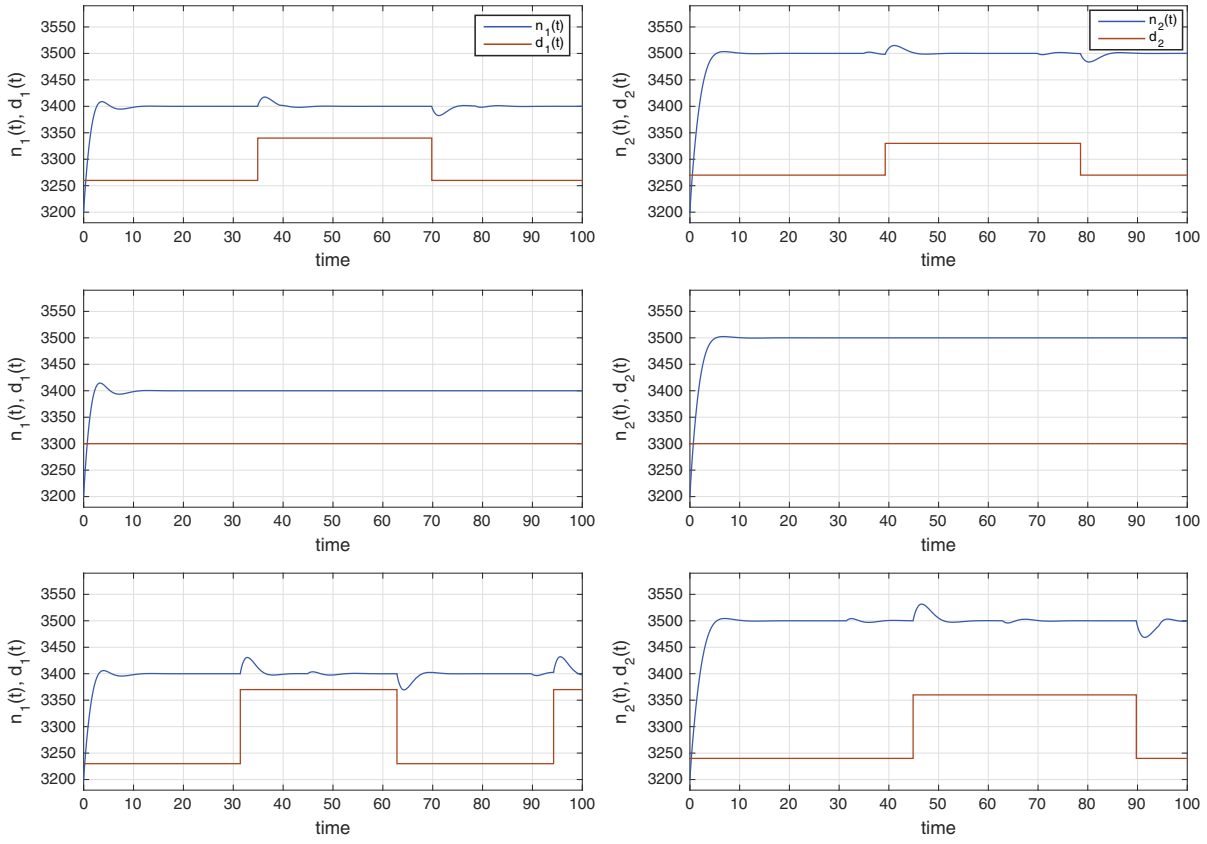

Fig. 6. Example 1b: reversed accumulation references, i.e. $n_1^* = 3400$ (veh) and $n_2^* = 3500$ (veh). Simulation of the adaptive control system for the model (21) with the plant coefficients (26) and the controllers (24), (25) with the parameters from Table 1. The graphs show the time history of the outputs $n_1(t), n_2(t)$ and the disturbances $d_1(t), d_2(t)$ for the two regions. The left subplots are the cases of $n_1^* = 3400$ and the right subplots are the cases of $n_2^* = 3500$. $n_o = 0.95 n_{cr}$, $\text{MFD}_1 = \text{MFD}_2 = \text{MFD}_{\text{Yok}}$, $n_1(0) = n_2(0) = 3200$ (veh).

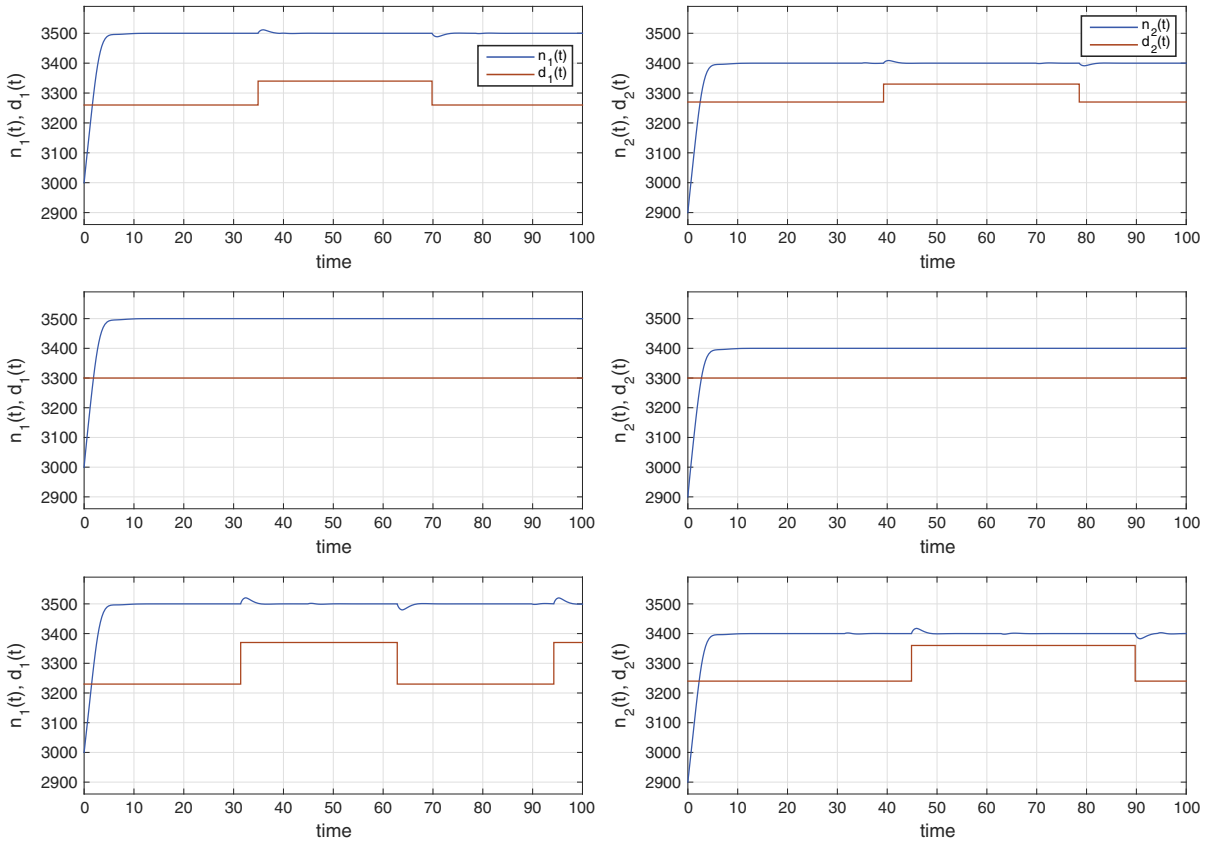

Fig. 7. Example 1c: different initial points $n_1(0) = 3000$ (veh) and $n_2(0) = 2900$ (veh). Simulation of the adaptive control system for the model (21) with the plant coefficients (26) and the controllers (24), (25) with the parameters from Table 1. The graphs show the time history of the outputs $n_1(t), n_2(t)$ and the disturbances $d_1(t), d_2(t)$ for the two regions. The left subplots are the cases of $n_1^* = 3500$ (veh) and the right subplots are the cases of $n_2^* = 3400$ (veh), $n_o = 0.95 n_{cr}$, $\text{MFD}_1 = \text{MFD}_2 = \text{MFD}_{\text{Yok}}$.

the performance efficiency of the adaptive perimeter controllers for other initial conditions, not similar to Examples 1a and 1b, under three variants of demand (disturbances).

Example 2. In Example 2, the performance of the adaptive controllers is tested for other operating points. Similar to Example 1, we also consider two identical models for both regions having the same MFD shapes, $\text{MFD}_1 = \text{MFD}_2 = \text{MFD}_{\text{Yok}}$, and the operating points for both regions are the same, but they are different from Example 1, determined as $n_o = 0.8 n_{cr} = 2720$ (veh). Hence, the coefficients of the plant (21) are also different, and given by

$$A_1 = A_2 = \begin{bmatrix} 0 & 1 \\ -28.7769 & -17.2950 \end{bmatrix}, \quad A_{12} = A_{21} = \begin{bmatrix} 0 & 0 \\ 5.7554 & 3.4590 \end{bmatrix}$$
$$b_1 = b_2 = [0 \quad 1]^T, \quad c_1 = c_2 = 1.0e+03 * [2.8771 \quad 0.1972]. \tag{27}$$

Moreover, both regions are initially uncongested with the same initial accumulations $n_1(0) = n_2(0) = 3200$ (veh).

Two cases are tested in Example 2. The simulation results of the adaptive control system for the model (21), with the plant coefficients (27), and the controllers (24), (25), with the parameters from Table 1, are shown in Figs. 8 and 9 for cases 2a and 2b, respectively. The results for each case illustrate the time response of the regional model outputs, i.e. $n_1(t)$ and $n_2(t)$, for the three different variants of disturbances $d_1(t), d_2(t)$. In cases 2a and 2b, we run the simulation for different accumulation references. The results in Fig. 8 are shown for the case 2a where the accumulation reference for region 1 is congested, i.e. $n_1^* = 3500$ (veh), and the accumulation reference for region 2 is equal to the critical accumulation $n_2^* = 3400$ (veh). While in Fig. 9, the results are shown for the reverse case, where the accumulation reference for region 1 is equal to the critical accumulation $n_1^* = 3400$ (veh), and the accumulation reference for region 2 is congested, i.e. $n_2^* = 3500$ (veh).

The results in Figs. 5 and 6 for Examples 1a and 1b, respectively, and in Figs. 8 and 9 for Examples 2a and 2b, respectively, show that the developed adaptive controllers perform well and satisfy the control specifications for different operating points under different disturbance variants and different accumulation references. There is no a noticeable difference in

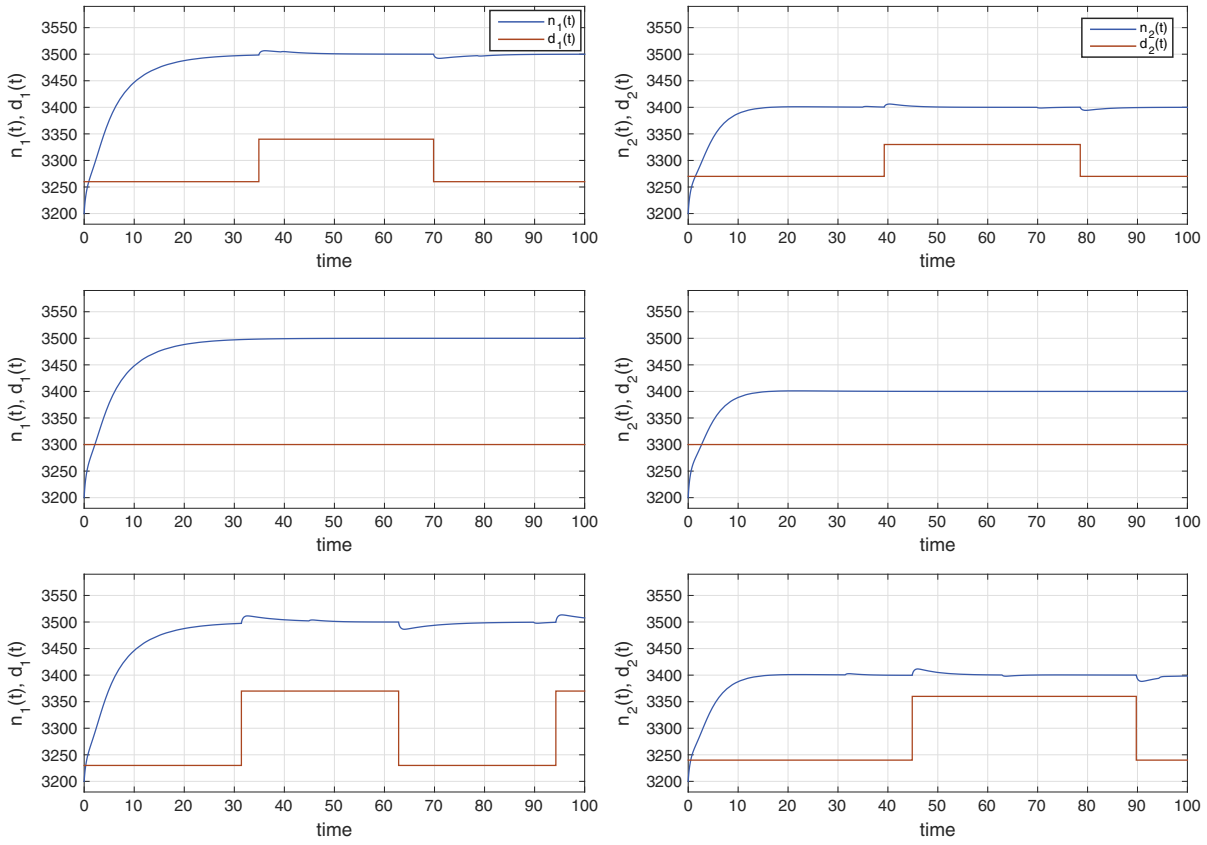

Fig. 8. Example 2a: simulation of the adaptive control system for the model (21) with the plant coefficients (27) and the controllers (24), (25) with the parameters from Table 1. The graphs show the time history of the outputs $n_1(t), n_2(t)$ and the disturbances $d_1(t), d_2(t)$ for the two regions. The left subplots are the cases of $n_1^* = 3500$ (veh) and the right subplots are the cases of $n_2^* = 3400$ (veh), $n_o = 0.8n_{cr}$, $\text{MFD}_1 = \text{MFD}_2 = \text{MFD}_{\text{Yok}}$, $n_1(0) = n_2(0) = 3200$.

the closed loop system behavior under a considerable change in the operating conditions. There are only little observable differences in the transient periods, since the adaptive controllers converge slower to the accumulation references when the references are far from the operating points.

Example 3. The performance of the adaptive perimeter controllers for the two urban regions with *different MFDs* is evaluated in Example 3. Two *nonidentical* models are considered for regions 1 and 2 with $\text{MFD}_1 = 0.6\text{MFD}_{\text{Yok}}$ and $\text{MFD}_2 = 1.4\text{MFD}_{\text{Yok}}$. The operating points for both regions are the same $n_o = 0.95n_{cr} = 3230$ (veh). The coefficients of the plant (21) are

$$A_1 = \begin{bmatrix} 0 & 1 \\ -4.6097 & -9.1876 \end{bmatrix}, \quad A_2 = \begin{bmatrix} 0 & 1 \\ -4.5521 & -15.8918 \end{bmatrix},$$
$$A_{12} = \begin{bmatrix} 0 & 0 \\ 1.2843 & 2.6586 \end{bmatrix}, \quad A_{21} = \begin{bmatrix} 0 & 0 \\ 0.9450 & 2.4540 \end{bmatrix},$$
$$b_1 = b_2 = [0 \quad 1]^T, \quad c_1 = [460.9144 \quad 51.7010], \quad c_2 = [454.9932 \quad 28.0860]. \tag{28}$$

The simulation results of the adaptive control system for the model (21), with the plant coefficients (28), and the controllers (24), (25), with the parameters from Table 1, are shown in Fig. 10. The results in Fig. 10 show that the desired performance is met for the two urban regions with different sizes of MFDs.

Example 4. The performance of the adaptive perimeter controllers for the three interconnected urban regions with *different MFDs* is evaluated in Example 4. Three *nonidentical* models are considered for regions 1, 2 and 3 with $\text{MFD}_1 = 0.6\text{MFD}_{\text{Yok}}, \text{MFD}_2 = 1.4\text{MFD}_{\text{Yok}}$ and $\text{MFD}_3 = \text{MFD}_{\text{Yok}}$.

The operating points, the matrices A_1, A_2, b_1, b_2 of the plant (22) and the disturbances $d_1(t), d_2(t)$ are the same as in Example 3 and the other parameters of (22) and (23) are

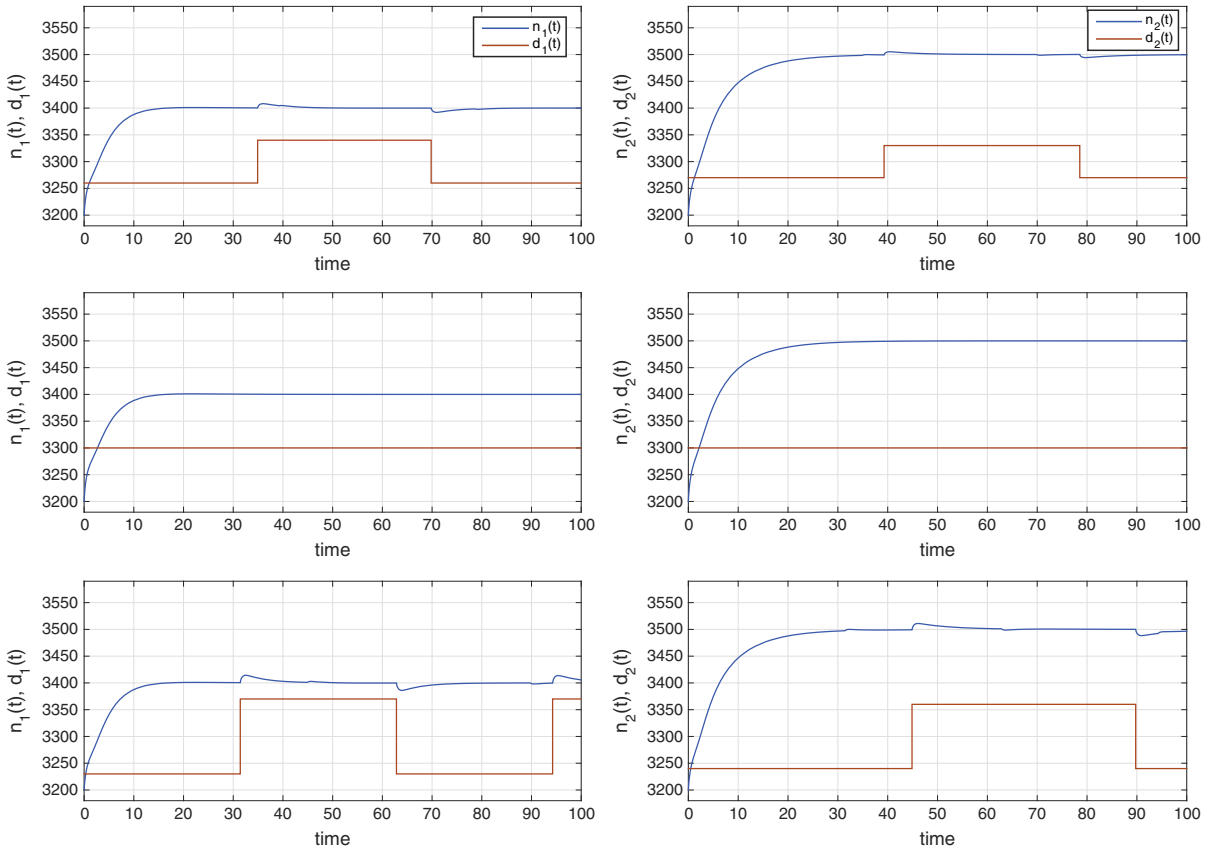

Fig. 9. Example 2b: simulation of the adaptive control system for the model (21) with the plant coefficients (27) and the controllers (24), (25) with the parameters from Table 1. The graphs show the time history of the outputs $n_1(t), n_2(t)$ and the disturbances $d_1(t), d_2(t)$ for the two regions. The left subplots are the cases of $n_1^* = 3400$ (veh) and the right subplots are the cases of $n_2^* = 3500$ (veh), $n_o = 0.8n_{cr}$, $\text{MFD}_1 = \text{MFD}_2 = \text{MFD}_{\text{Yok}}$, $n_1(0) = n_2(0) = 3200$ (veh).

$$A_3 = \begin{bmatrix} 0 & 1 & 0 \\ 0 & 0 & 1 \\ -25.8743 & -58.764 & -13.894 \end{bmatrix}, \quad A_{r3} = \begin{bmatrix} 0 & 1 & 0 \\ 0 & 0 & 1 \\ -30 & -140 & -60 \end{bmatrix},$$

$$A_{13} = \begin{bmatrix} 0 & 0 & 0 \\ 0 & 0 & 0 \\ 2.9312 & 2.4230 & 3.9433 \end{bmatrix}, \quad A_{23} = \begin{bmatrix} 0 & 0 & 0 \\ 0 & 0 & 0 \\ 0.8432 & 2.3218 & 0.5435 \end{bmatrix},$$

$$A_{31} = \begin{bmatrix} 0 & 0 \\ 0 & 0 \\ 0.3642 & 2.2682 \end{bmatrix}, \quad A_{32} = \begin{bmatrix} 0 & 0 \\ 0 & 0 \\ 2.7131 & 9.1242 \end{bmatrix},$$

$$b_3 = b_{r3} = [0 \quad 0 \quad 1]^T, \quad d_3(t) = 40 + 80\text{Square}(0.07t) \text{ (rad/s)}. \tag{29}$$

Note that in this example, the magnitude of the perturbation in the region 3 is greater than the magnitude in the region 1 in 2 times, and in 1.6 times than the magnitude in the region 2.

The simulation results of the adaptive control system for the model (22), with the plant coefficients (29), and the controllers (24), (25), with the controller parameters from Table 1 and $k_{P3} = k_{P1}, k_{I3} = k_{I1}, k_{D3} = k_{D1}, \gamma_3 = \gamma_1$,

$$P_3 = \begin{bmatrix} 9.5259 & 6.5517 & 0.0833 \\ 6.5517 & 12.7830 & 0.1509 \\ 0.0833 & 0.1509 & 0.1767 \end{bmatrix},$$

are shown in Fig. 11. The results in Fig. 11 show that the desired performance is met for the three urban regions with different sizes of MFDs.

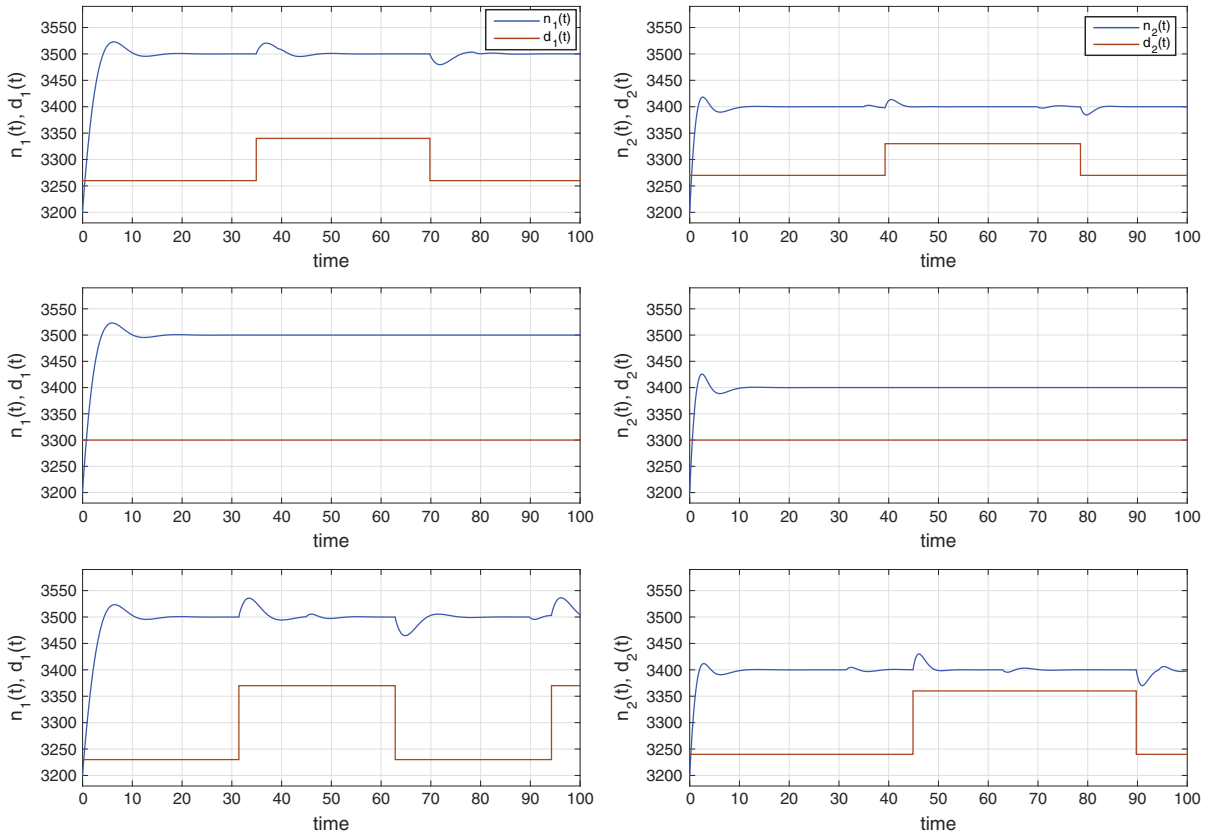

Fig. 10. Example 3: different MFDs for regions 1 and 2, i.e. $\mathrm{MFD}_1 = 0.6\mathrm{MFD}_{\mathrm{Yok}}; \mathrm{MFD}_2 = 1.4\mathrm{MFD}_{\mathrm{Yok}}$. Simulation of the adaptive control system for the model (21) with the plant coefficients (28) and the controllers (24), (25) with the parameters from Table 1. The graphs show the time history of the outputs $n_1(t), n_2(t)$ and the disturbances $d_1(t), d_2(t)$ for the two regions. The left subplots are the cases of $n_1^* = 3500$ (veh) and the right subplots are the cases of $n_2^* = 3400$ (veh), $n_o = 0.95 n_{cr}$, $n_1(0) = n_2(0) = 3200$ (veh).

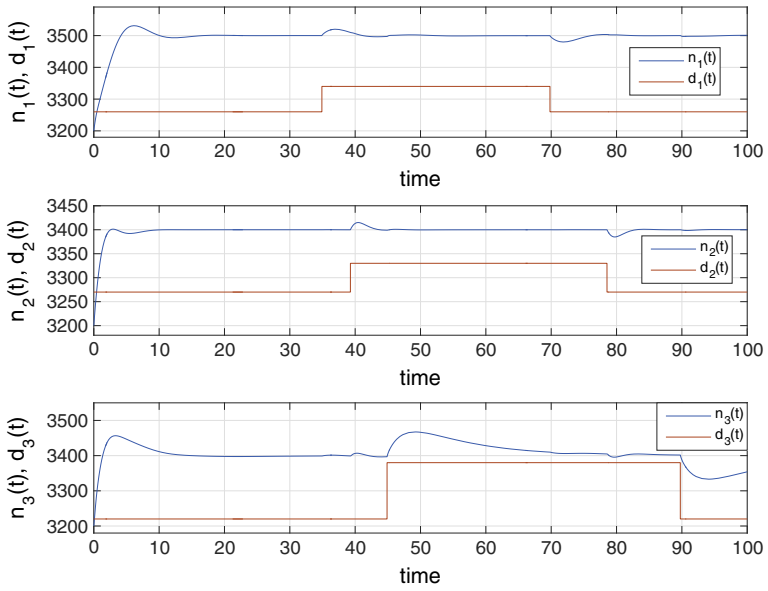

Fig. 11. Example 4: different MFDs for regions 1, 2 and 3, i.e. $\mathrm{MFD}_1 = 0.6\mathrm{MFD}_{\mathrm{Yok}}; \mathrm{MFD}_2 = 1.4\mathrm{MFD}_{\mathrm{Yok}}, \mathrm{MFD}_3 = \mathrm{MFD}_{\mathrm{Yok}}$. Simulation of the adaptive control system for the model (22) with the plant coefficients (29) and the controllers (24), (25). The graphs show the time history of the outputs $n_1(t), n_2(t), n_3(t)$ and the disturbances $d_1(t), d_2(t), d_3(t)$ for the three regions.

5. Conclusions and future work

A distributed adaptive perimeter (DAP) control design at multi-region networks has been presented. The concept of the macroscopic fundamental diagram (MFD) has been utilized for modeling the traffic flow dynamics at multi-region networks. First, the MFD-based model has been formulated in an interconnected form, then the reference model coordination approach has been developed to allow us designing DAP control laws. The developed adaptive control scheme postulates one controller structure, however, the controllers' gains vary with time to adapt themselves against the model parameter uncertainties. Lyapunov-Krasovskii functionals are used to prove stability and exact asymptotic tracking for the DAP control laws.

The DAP controllers were shown to be efficient for different conditions by numerical examples. The results show that the developed DAP controllers can bring initial accumulations to desired accumulations that are not necessary equal to the operating points. Moreover, the performance of the DAP controllers has been tested for different operating points and different shapes of MFDs under different demand disturbance variants and different accumulation references. In all numerical examples, the outputs or regional accumulations in the adaptive control system are bounded, and the desired tracking performance is met.

The results demonstrate the flexibility of the DAP controllers in handling different cases and various traffic situations. This work is considered as another step forward towards enhanced perimeter control strategies in general, and achieving DAP control structure for transportation networks based on MFD in particular.

This research answers the question whether individual regions can exactly track their desired accumulations (outputs), without any information concerning the other regions. Theorem 1 states and the numerical results obtained show that this is indeed possible provided each region is aware of the desired accumulations of the other regions. This can be done with the help of coordination, e.g. a large-scale traffic management center coordinates between regional traffic control centers. Note that the accumulation references can be a priori given constant accumulation points, or accumulation trajectories which might vary with time. In the case of multiple regions, it is clear that in some cases, e.g. when a network is heavily congested, the controllers might not succeed to regulate around all reference accumulation points, or sometimes the reference points should be changed during the control process. The accumulation references of the different approaches presented in Haddad (2015) and Haddad and Shraiber (2014) are assumed to be *constant* accumulations, and the designed robust controllers should regulate around them. The design approach utilized in this paper can handle not only constant accumulation references, but it also allows the control design for arbitrary desired time-varying behavior, which can be realized by tracking a *desired time function*. A future research would be to synthesize DAP controllers for desired time-varying accumulations. However, before conducting this, another future research should focus on deriving the *optimal accumulation references*, i.e. constant or time-varying accumulations, of a network with multiple regions.

Further research is needed to investigate what type of networks might not be appropriate for MFD-based modeling and control, e.g. Saberi and Mahmassani (2012) and Geroliminis and Sun (2011a) have shown that MFD might experience hysteresis loops for freeway networks. It should be stressed that urban networks without redundant characteristics, e.g. not many possible route choices for most O-D pairs, and very heterogeneous distribution of congestion, i.e. non-partitionable in more homogeneous regions, might not have well-defined MFDs. The concept of uncertain MFD with interval function, i.e. nominal MFD values with upper and lower bounds, as has been presented in this paper, aims to tackle scatter MFDs and to make the MFD-based models appropriate for MFD control.

Acknowledgements

This research was supported by the Israel Science Foundation (ISF Grant No. 0251502).

Appendix A. Proof of Theorem 1

As it is generally done in traditional model reference adaptive control (MRAC), see e.g. Ioannou and Sun (1996), Tao (2003), the following assumptions are made on the system model (11) and the reference models (12): (A1) There exist *unknown* constant matrices $\theta^*_{xi} \in \mathbb{R}^{(1+card(S_i))\times card(S_i)}$ and $\theta^*_{ri} = diag\{\theta^*_{r1}, \ldots, \theta^*_{rk}, \ldots, \theta^*_{card(S_i)}\} \in \mathbb{R}^{card(S_i)\times card(S_i)}$ such that the following equations are satisfied:

$$A_i + B_i\theta^{*T}_{xi} = A_{ri}, \quad B_i = B_{ri}\theta^*_{ri}, \tag{A.1}$$

(A2) there exists a matrix S_{pi} such that $\theta^*_{ri}S_{pi} = (\theta^*_{ri}S_{pi})^T > 0$, (A3) the external disturbance $d_i(t)$ and the nonlinear perturbations $p_{ij}(x_j(t))$ are bounded by *unknown* positive constants, that is $\|d_i(t)\| \leqslant d^*_i$ and $\|p_{ij}(x_j(t))\| \leqslant p^*_{ij}$, and (A4) $A_{ij} = B_i\theta^{*T}_{ij}$, where the constant matrix $\theta^*_{ij} \in \mathbb{R}^{(1+card(S_j))\times card(S_i)}$ is *unknown*.

Firstly in view of (11), (12) and the assumption (A1), we express the closed-loop system in terms of the tracking error $e_i(t) = x_i(t) - x_{ri}(t)$

$$\dot{e}_i(t) = A_{ri}e_i(t) - B_i\theta^{*T}_i e_i(t) + B_iu_i(t) - B_{ri}r_i(t) + B_id_i(t) + \sum_{j\in S_i} B_i\theta^{**T}_{ij}x_{rj} + \sum_{j\in S_i} B_i\theta^{*T}_{ij}e_j(t) + \sum_{j\in S_i} B_ip_{ij}(x_j(t)), \tag{A.2}$$

where

$$\theta_{ij}^{**} = \begin{cases} \theta_{ij}^{*} & \text{if } i \neq j, \\ \theta_{ii}^{*} + \theta_{i}^{*} & \text{if } i = j. \end{cases}$$

Then introducing the parameter errors $\tilde{\theta}_i(t) = \theta_i(t) - \theta_i^*$ and $\tilde{\theta}_{ij}(t) = \theta_{ij}(t) - \theta_{ij}^{**}$ and using (14) and (16), we obtain from (A.2) the following basic tracking error equation

$$\begin{aligned} \dot{e}_i(t) = {} & A_{ri}e_i(t) + B_{ri}\theta_{ri}^{*}\tilde{\theta}_i^T(t)e_i(t) + \sum_{j\in S_i} B_{ri}\theta_{ri}^{*}\tilde{\theta}_{ij}^T(t)x_{rj}(t) + B_{ri}\theta_{ri}^{*}u_{li}(t) - B_{ri}r_i(t) + B_{ri}\theta_{ri}^{*}d_i(t) + \sum_{j\in S_i} B_{ri}\theta_{ri}^{*}\theta_{ij}^{*T}e_j(t) \\ & + B_{ri}\theta_{ri}^{*}d_i(t) + \sum_{j\in S_i} B_{ri}\theta_{ri}^{*}p_{ij}(x_j(t)). \end{aligned} \tag{A.3}$$

Now we define a Lyapunov-Krasovskii type functional V as

$$\begin{aligned} V &= \sum_{i=1}^{R}\left[V_{ei} + V_{\alpha i} + V_{\eta i} + V_{\eta ij}\right], \\ V_{ei} &= e_i^T P_i e_i, \\ V_{\eta i} &= \frac{1}{\gamma_i}\mathrm{tr}\left(\tilde{\eta}_i\Gamma_i\tilde{\eta}_i^T + \int_{t-h_i}^{t}\eta_i(s)\Gamma_i\eta_i^T(s)ds\right), \\ V_{\eta ij} &= \sum_{j\in S_i}\frac{1}{\gamma_{ij}}\mathrm{tr}\left(\tilde{\eta}_{ij}(t)\Gamma_i\tilde{\eta}_{ij}^T(t) + \int_{t-h_{ij}}^{t}\eta_{ij}(s)\Gamma_i\eta_{ij}^T(s)ds\right), \\ V_{\alpha i} &= \sum_{k=1}^{card(S_i)}|\theta_{rik}^{*}|\gamma_{ik}^{-1}\tilde{\alpha}_{ik}^2(t), \end{aligned} \tag{A.4}$$

where

$$\begin{aligned} \tilde{\eta}_i &= \tilde{\theta}_i(t) + \eta_i^* + \eta_i(t) + \eta_i(t-h_i), \\ \tilde{\eta}_{ij} &= \tilde{\theta}_{ij}(t) + \eta_{ij}(t) + \eta_{ij}(t-h_{ij}), \\ \tilde{\alpha}_i(t) &= \alpha_{ik}(t) - \alpha_{ik}^{*}\mathrm{sgn}(E_{ik}), \end{aligned} \tag{A.5}$$

$\Gamma_i = \theta_{ri}^{*T}S_{pi}^{-1}$, the known matrix S_{pi} satisfies $\theta_{ri}^{*}S_{pi} = (\theta_{ri}^{*}S_{pi})^T > 0$, see (A2), $\gamma_i > 0, \gamma_{ij} > 0, h_i > 0$ and $h_{ij} > 0$ are some design parameters and η_i^* is an as yet unspecified positive constant vector. The sign function is defined as $\mathrm{sgn}(\star) = 1$, if $(\star) > 0$; $\mathrm{sgn}(\star) = 0$, if $(\star) = 0$;; $\mathrm{sgn}(\star) = -1$, if $(\star) < 0$. The component η_i^* and the unknown scalar α_{ik}^* are "artificial" and used only in the process of the stability proof. The scalar "virtual" adaptation gain $\alpha_{ik}(t)$ and the scalar constants α_{ik}^* will be defined latter.

Using (15), the time derivatives of the components of (A.4) along (A.3) can be written as

$$\begin{aligned} \dot{V}_{ei}|_{(A.3)} = {} & -e_i^T(t)Q_ie_i(t) + \sum_{j\in S_i}2e_i^TP_iB_{ri}\theta_{ri}^{*}\theta_{ij}^{*}e_j(t) + 2e_i^TP_iB_{ri}\theta_{ri}^{*}u_{li}(t) + \mathrm{tr}\left(e_i(t)e_i^T(t)P_iB_{ri}\theta_{ri}^{*}\tilde{\theta}_i^T\right) \\ & + \mathrm{tr}\left(\tilde{\theta}_i\theta_{ri}^{*T}B_{ri}^TP_ie_i(t)e_i^T(t)\right) + \sum_{j\in S_i}\mathrm{tr}\left(x_je_i^TP_{ri}B_{ri}\theta_{ri}^{*}\tilde{\theta}_{ij}^T\right) + \sum_{j\in S_i}\mathrm{tr}\left(\tilde{\theta}_{ij}\theta_{ri}^{*T}B_i^TP_ie_ix_j^T\right) + 2e_i^TP_iB_{ri}\left(r_i(t) + \theta_{ri}^{*}d_i(t)\right) \\ & + 2e_i^TP_iB_{ri}\sum_{j\in S_i}\theta_{ri}^{*}p_{ij}(x_j(t)), \end{aligned} \tag{A.6}$$

$$\begin{aligned} \dot{V}_{\eta i}|_{(A.3)} = {} & -\mathrm{tr}\left([\eta_i(t) + \eta_i(t-h_i)]\Gamma_i[\eta_i(t) + \eta_i(t-h_i)]^T\right) - \mathrm{tr}\left(\eta_i(t)\Gamma_i\tilde{\theta}_{fi}^T(t) + \tilde{\theta}_{fi}(t)\Gamma_i\eta_i^T(t)\right) \\ & - \mathrm{tr}\left(\eta_i(t)\Gamma_i\eta_i^{*T} + \eta_i^*\Gamma_i\eta_i^T(t)\right), \end{aligned} \tag{A.7}$$

$$\dot{V}_{\eta ij}|_{(A.3)} = -\mathrm{tr}[\eta_{ij}(t) + \eta_{ij}(t-h_{ij})]\Gamma_i[\eta_{ij}(t) + \eta_{ij}(t-h_{ij})]^T - \mathrm{tr}\left(\eta_{ij}(t)\Gamma_i\tilde{\theta}_{ij}^T(t) + \tilde{\theta}_{ij}(t)\Gamma_i\eta_{ij}^T(t)\right). \tag{A.8}$$

Let us now choose

$$\eta_i^{*T} = [\frac{1}{2}\theta_{ri}^{*-1}\overline{Q}_i\,0\ldots0], \qquad \overline{Q}_i = \overline{Q}_i^T > 0. \tag{A.9}$$

Then, in view of Eqs. (17) and (15), we get for the last terms of (A.7)

$$\mathrm{tr}\left(\eta_i(t)\Gamma_i\eta_i^{*T} + \eta_i^*\Gamma_i\eta_i^T(t)\right) = e_i^TP_i^TB_i\overline{Q}_iB_i^TP_ie_i. \tag{A.10}$$

Remark 6. This term, (A.10), aids the proof and does not influence the control value.

Now we define the "virtual" adaptation gains $\alpha_{ik}(t)$ in (A.4) as

$$\dot{\alpha}_{ik}(t) = -\gamma_{ik}E_{ik}(t), \quad \alpha_{ik}(0) = 0 \tag{A.11}$$

and by using (A.11) we compute the time derivative of $V_{\alpha i}$ for two cases - when $E_{ik}(t) \neq 0$ and $E_{ik}(t) = 0$.

$$\begin{aligned}
&\dot{V}_{\alpha i}|_{(A.3)}^{E_{ik}\neq 0} = -\sum_{k=1}^{card(S_i)} 2\theta_{rik}^{*}\tilde{\alpha}_{ik}(t)\int_0^t E_{ik}(t)\mathrm{d}t,\\
&\dot{V}_{\alpha i}|_{(A.3)}^{S_i=0} = 0.
\end{aligned} \tag{A.12}$$

Further using (A.6)–(A.8), dropping negative terms and exploiting (17), (A.9) and (A.10), it can be shown that the time derivative of $V_{1i} = V_{ei} + V_{\eta i} + V_{\eta ij}$ along the error Eq. (A.3) is given by

$$\begin{aligned}
\dot{V}_{1i}|_{(A.3)} \leqslant &\sum_{i=1}^{R}\left[-e_i^T(t)Q_ie_i(t) + 2e_i^TP_iB_{ri}\theta_{ri}^{*}u_{li}(t) + 2e_i^TP_iB_{ri}r_i(t) + 2e_i^TP_iB_{ri}\theta_{ri}^{*}d_i(t) + 2e_i^TP_iB_{ri}\sum_{j\in S_i}\theta_{ri}^{*}p_{ij}(x_j(t))\right]\\
&+\sum_{i=1}^{R}\sum_{j\in S_i} -\frac{r_0}{M}e_i^TP_i^TB_{ri}B_{ri}^TP_ie_i + 2e_i^T(t)P_iB_{ri}\theta_{ri}^{*}\theta_{ij}^{*}e_j(t),
\end{aligned} \tag{A.13}$$

where $M = card(S_i) > 0$ and we assigned $\overline{Q}_i$ as $r_0 > 0$.

Complementing to squares and dropping the negative term, we have the following estimation for the last term of (A.13)

$$\begin{aligned}
&\sum_{i=1}^{R}\sum_{j\in S_i} -\frac{r_0}{M}e_i^TP_i^TB_{ri}B_{ri}^TP_ie_i + 2e_i^T(t)P_iB_{ri}\theta_{ri}^{*}\theta_{ij}^{*}e_j(t)\\
&\leqslant \frac{M}{r_0}\sum_{i=1}^{R}\sum_{j\in S_i}e_i^T(t)\Psi_{ji}e_i(t), \quad \Psi_{ji} = \theta_{ji}^{*T}\theta_{rj}^{*T}\theta_{rj}^{*}\theta_{ji}^{*}
\end{aligned} \tag{A.14}$$

By using the inequality from (A3) and boundedness of the reference signal $r_i(t)$ ($\|r_i(t)\| \leqslant r_i^{*}$, $r_i^{*} > 0$) and $\|p_{ij}(x_j(t))\| \leqslant p_{ij}^{*}$, we can write the following estimates of the terms of (A.13)

$$\begin{aligned}
&2e_i^T(t)P_iB_{ri}r_i(t) \leqslant \|e_i^T(t)P_iB_{ri}r_i(t)\|_1 \leqslant \sum_{k=1}^{card(S_i)}|E_{ik}(t)|r_{ik}^{*}\\
&2e_i^T(t)P_iB_{ri}\theta_{ri}^{*}d_i(t) \leqslant \|e_i^T(t)P_iB_{ri}\theta_{ri}^{*}d_i(t)\|_1 \leqslant \sum_{k=1}^{card(S_i)}|E_{ik}(t)|\theta_{rik}^{*}d_{ik}^{*}\\
&2e_i^TP_iB_{ri}\sum_{j\in S_i}\theta_{ri}^{*}p_{ij}(x_j(t)) \leqslant \|e_i^T(t)P_iB_{ri}\|_1\sum_{j\in S_i}\|\theta_{ri}^{*}p_{ij}(x_j(t))\| \leqslant \sum_{k=1}^{card(S_i)}|E_{ik}(t)|\bar{p}_i^{*}
\end{aligned} \tag{A.15}$$

where $\|\bigstar\|_1$ is a sign of the 1-norm, $\bar{p}_i^{*} = \sum_{j\in S_i}\|\theta_{ri}^{*}\|p_{ij}^{*}$ and $E_{ik}(t)$ is the k-th element of the vector $e_i^T(t)P_iB_{ri}$, see (14). Applying (A.14) and (A.15) to (A.13) yields

$$\dot{V}_{1i}|_{(A.3)} \leqslant \sum_{i=1}^{R}\left[-e_i^T(t)Q_ie_i(t) + 2e_i^TP_iB_{ri}\theta_{ri}^{*}u_{li}(t) + \sum_{k=1}^{card(S_i)}|E_{ik}(t)|\alpha_{ik}^{*} + \frac{M}{r_0}\sum_{j\in S_i}e_i^T(t)\Psi_{ji}e_i(t)\right], \tag{A.16}$$

where $\alpha_{ik}^{*} = -(r_{ik}^{*} + d_{ik}^{*} + \bar{p}_i^{*})$.

For convenience, let Q_i from (A.13) be $Q_i = (Q_{1i} + Q_{2i}), Q_{1i} = Q_{1i}^T > 0$ and $Q_{2i} = Q_{2i}^T > 0$. Then by selecting the value r_0 from the inequality

$$r_0\lambda_{min}(Q_{2i}) > \lambda_{max}(\Psi_{ji}), \tag{A.17}$$

where $\lambda_{min}(\bigstar)$ and $\lambda_{max}(\bigstar)$ are the minimum and maximum eigenvalues of $(\bigstar)$ respectively, we obtain from (A.16)

$$\dot{V}_{1i}|_{(A.3)} \leqslant \sum_{i=1}^{R}\left[-e_i^T(t)Q_{1i}e_i(t) + 2e_i^TP_iB_{ri}\theta_{ri}^{*}u_{li}(t) + \sum_{k=1}^{card(S_i)}|E_{ik}(t)|\alpha_{ik}^{*}\right]. \tag{A.18}$$

Applying (A.12), (A.18) and the control component $u_{lik}(t)$ from (14) to (A.4) after simplifications we obtain

$$\dot{V}|_{(A.3)} \leqslant \sum_{i=1}^{R} -e_i^T(t)Q_{1i}e_i(t). \tag{A.19}$$

This implies that V and, therefore $e_i(t), \tilde{\theta}_i(t), \theta_i(t), \tilde{\theta}_{ij}(t), \theta_{ij}(t), \tilde{\alpha}_i(t), \alpha_i(t) \in L_\infty, (i = 1, \ldots, R; j \in S_i)$ and $e_i(t) \in L_2$ by following the usual arguments Ioannou and Sun (1996). Then it follows from (14) and (16) that $u_i(t) \in L_\infty$. Furthermore, $x_{ri}(t), e_i(t) \in L_\infty$ imply that $x_i(t) \in L_\infty$. In view of (A.3) also $\dot{e}_i(t) \in L_\infty$. With $e_i(t) \in L_2 \bigcap L_\infty$ and $\dot{e}_i(t) \in L_\infty$, applying, e.g. Corollary 2.8. (Tao, 2003 p.81), we conclude that $\lim_{t\to\infty} e_i(t) = 0$ for all $i = 1, \ldots, R$.

So we have shown that the local states $x_i(t)$ asymptotically track the states $x_{ri}(t)$ of the autonomous reference models, and therefore, the local outputs $y_i(t)$ asymptotically track the reference model outputs $y_{ri}(t)$. The reference model dynamics can be chosen such that the local outputs $y_i(t)$ track specified external signals e.g. constants.

References

Aboudolas, K., Geroliminis, N., 2013. Perimeter and boundary flow control in multi-reservoir heterogeneous networks. Transport. Res. Part B 55, 265–281.
Buisson, C., Ladier, C., 2009. Exploring the impact of homogeneity of traffic measurements on the existence of macroscopic fundamental diagrams. Transport. Res. Rec. 2124, 127–136.
Daganzo, C.F., 2007. Urban gridlock: macroscopic modeling and mitigation approaches. Transport. Res. Part B 41 (1), 49–62.
Daganzo, C.F., Gayah, V.V., Gonzales, E.J., 2011. Macroscopic relations of urban traffic variables: bifurcations, multivaluedness and instability. Transport. Res. Part B 45 (1), 278–288.
Gayah, V.V., Daganzo, C.F., 2011a. Clockwise hysteresis loops in the macroscopic fundamental diagram: an effect of network instability. Transport. Res. Part B 45 (4), 643–655.
Gayah, V.V., Daganzo, C.F., 2011b. Exploring the effect of turning maneuvers and route choice on a simple network. Transport. Res. Rec. 2249, 15–19.
Geroliminis, N., Daganzo, C.F., 2008. Existence of urban-scale macroscopic fundamental diagrams: some experimental findings. Transport. Res. Part B 42 (9), 759–770.
Geroliminis, N., Haddad, J., Ramezani, M., 2013. Optimal perimeter control for two urban regions with macroscopic fundamental diagrams: a model predictive approach. IEEE Trans. Intell. Transport. Syst. 14 (1), 348–359.
Geroliminis, N., Sun, J., 2011a. Hysteresis phenomena of a macroscopic fundamental diagram in freeway networks. Transport. Res. Part A 45 (9), 966–979.
Geroliminis, N., Sun, J., 2011b. Properties of a well-defined macroscopic fundamental diagram for urban traffic. Transport. Res. Part B 45 (3), 605–617.
Godfrey, J.W., 1969. The mechanism of a road network. Traffic Eng. Control 11 (7), 323–327.
Haddad, J., 2015. Robust constrained control of uncertain macroscopic fundamental diagram networks. Transport. Res. Part C 59, 323–339.
Haddad, J., 2017. Optimal perimeter control synthesis for two urban regions with aggregate boundary queue dynamics. Transport. Res. Part B 96, 1–25.
Haddad, J., Geroliminis, N., 2012. On the stability of traffic perimeter control in two-region urban cities. Transport. Res. Part B 46 (1), 1159–1176.
Haddad, J., Mirkin, B., 2016. Adaptive perimeter traffic control of urban road networks based on MFD model with time delays. Int. J. Nonlinear Robust Control 26 (6), 1267–1285 (Special Issue on "Recent Trends in Traffic Modelling and Control).
Haddad, J., Ramezani, M., Geroliminis, N., 2013. Cooperative traffic control of a mixed network with two urban regions and a freeway. Transport. Res. Part B 54, 17–36.
Haddad, J., Shraiber, A., 2014. Robust perimeter control design for an urban region. Transport. Res. Part B 68, 315–332.
Hajiahmadi, M., Haddad, J., Schutter, B.D., Geroliminis, N., 2015. Optimal hybrid perimeter and switching plans control for urban traffic networks. IEEE Trans. Control Syst. Technol. 23 (2), 464–478.
Ioannou, P.A., Sun, J., 1996. Robust Adaptive Control. Prentice Hall, New Jersey.
Ji, Y., Daamen, W., Hoogendoorn, S., Hoogendoorn-Lanser, S., Qian, X., 2010. Macroscopic fundamental diagram: investigating its shape using simulation data. Transport. Res. Rec. 6121, 42–48.
Ji, Y., Geroliminis, N., 2012. On the spatial partitioning of urban transportation networks. Transport. Res. Part B 46 (10), 1639–1656.
Ji, Y., Luo, J., Geroliminis, N., 2014. Empirical observations of congestion propagation and dynamic partitioning with probe data for large scale systems. Transport. Res. Rec. 2422 (2), 1–11.
Keyvan-Ekbatani, M., Kouvelas, A., Papamichail, I., Papageorgiou, M., 2012. Exploiting the fundamental diagram of urban networks for feedback-based gating. Transport. Res. Part B 46 (10), 1393–1403.
Keyvan-Ekbatani, M., Papageorgiou, M., Knoop, V., 2015. Controller design for gating traffic control in presence of time-delay in urban road networks. Transport. Res. Part C 59, 308–322.
Keyvan-Ekbatani, M., Papageorgiou, M., Papamichail, I., 2013. Urban congestion gating control based on reduced operational network fundamental diagrams. Transport. Res. Part C, 74–87.
Knoop, V., Hoogendoorn, S., van Lint, H., 2013. The impact of traffic dynamics on the macroscopic fundamental diagram. In: 92nd Annual Meeting of Transportation Research Board, Washington D.C., USA.
Knoop, V.L., Hoogendoorn, S.P., Van Lint, J.W.C., 2012. Routing strategies based on the macroscopic fundamental diagram. Transport. Res. Rec. 2315, 1–10.
Kouvelas, A., Lioris, J., Fayazi, S., Varaiya, P., 2014. Maximum pressure controller for stabilizing queues in signalized arterial networks. Transport. Res. Rec.: J. Transport. Res. Board (2421), 133–141.
Kumar, V., Leonard, N., Morse, A. (Eds.), 2005. Cooperative Controls. Springer-Verlag, Berlin, Heidelberg.
Laval, J.A., Castrillón, F., 2015. Stochastic approximations for the macroscopic fundamental diagram of urban networks. Transport. Res. Part B 81, 904–916.
Leclercq, L., Chiabaut, N., Trinquier, B., 2014. Macroscopic fundamental diagrams: a cross-comparison of estimation methods. Transport. Res. Part B, 1–12.
Leclercq, L., Parzani, C., Knoop, V.L., Amourette, J., Hoogendoorn, S., 2015. Macroscopic traffic dynamics with heterogeneous route patterns. Transport. Res. Part C 59, 292–307.
Mahmassani, H., Williams, J., Herman, R., 1987. Performance of urban traffic networks. In: Gartner, N., Wilson, N. (Eds.), Proceedings of the 10th International Symposium on Transportation and Traffic Theory. Elsevier, Amsterdam, The Netherlands.
Mahmassani, H.S., Saberi, M., Zockaie, A.K., 2013. Urban network gridlock: theory, characteristics, and dynamics. Transport. Res. Part C 36, 480–497.
Mazloumian, A., Geroliminis, N., Helbing, D., 2010. The spatial variability of vehicle densities as determinant of urban network capacity. Philos. Trans. Roy. Soc. A: Math. Phys. Eng. Sci. 368 (1928), 4627–4647.
Mirkin, B., Gutman, P.-O., Shtessel, Y., 2012. Coordinated decentralized sliding mode MRAC with control cost optimization for a class of nonlinear systems. J. Franklin Inst. 349, 1364–1379.
Mirkin, B., Haddad, J., Shtessel, Y., 2016. Tracking with asymptotic sliding mode and adaptive input delay effect compensation of nonlinearly perturbed delayed systems applied to traffic feedback control. Int. J. Control. 89 (9), 1890–1903.
Mirkin, B.M., 2003. Comments on "Exact output tracking in decentralized adaptive control". IEEE Trans. Autom. Control 48 (2), 348–350.
Mirkin, B.M., Gutman, P.O., 2003. Decentralized output-feedback MRAC of linear state delay systems. IEEE Trans. Autom. Control 48 (9), 1613–1619.
Mirkin, B.M., Gutman, P.-O., 2010. Robust adaptive output-feedback tracking for a class of nonlinear time-delayed plants. IEEE Trans. Autom. Control 55 (10), 2418–2424.
Olszewski, P., Fan, H.S.L., Tan, Y.-W., 1995. Area-wide traffic speed-flow model for the Singapore CBD. Transport. Res. Part A 29A (4), 273–281.
Ortigosa, J., Menendez, M., Tapia, H., 2014. Study on the number and location of measurement points for an mfd perimeter control scheme: a case study of Zurich. EURO J. Transport. Logist. 3 (3–4), 245–266.
Ramezani, M., Haddad, J., Geroliminis, N., 2015. Dynamics of heterogeneity in urban networks: aggregated traffic modeling and hierarchical control. Transport. Res. Part B 74, 1–19.

Saberi, M., Mahmassani, H., 2012. Exploring properties of network-wide flow-density relations in a freeway network. In: Transportation Research Board 91st Annual Meeting, Washington, D.C.
Smith, M.J., 1980. A local traffic control policy which maximizes the overall travel capacity of an urban road network. Traffic Eng. Control 21 (6), 11–31.
Smith, M.J., Mounce, R., 2011. A splitting rate model of traffic re-routeing and traffic control. Transport. Res. Part B 45, 1389–1409.
Tao, G., 2003. Adaptive Control Design and Analysis. John Wiley & Sons, New York.
Tarbouriech, S., Abdallah, C., Chiasson, J. (Eds.), 2005. Advances in Communication Control Networks. Springer-Verlag, Berlin, Heidelberg.
Varaiya, P., 2013. Max pressure control of a network of signalized intersections. Transport. Res. Part C: Emerg. Technol. 36, 177–195.
Šiljak, D.D., 1991. Decentralized control of complex systems. Academic Press, Boston, MA.
Xiong, C., Chen, X., He, X., Lin, X., Zhang, L., 2016. Agent-based en-route diversion: dynamic behavioral responses and network performance represented by macroscopic fundamental diagrams. Transport. Res. Part C 64, 148–163.
Xue, Z., Chiabaut, N., Leclercq, L., 2016. Evaluation of the effect of traffic modeling on the control of traffic networks. In: Transportation Research Board 95th Annual Meeting, No. 16-2205.
Yildirimoglu, M., Geroliminis, N., 2014. Approximating dynamic equilibrium conditions with macroscopic fundamental diagrams. Transport. Res. Part B: Methodol. 70, 186–200.
Yildirimoglu, M., Ramezani, M., Geroliminis, N., 2015. Equilibrium analysis and route guidance in large-scale networks with mfd dynamics. Transport. Res. Part C 59, 404–420.
Zhang, L., Garoni, T., de Gier, J., 2013. A comparative study of macroscopic fundamental diagrams of arterial road networks governed by adaptive traffic signal systems. Transport. Res. Part B 49, 1–23.
Zhang, Z., Wolshon, B., Dixit, V.V., 2015. Integration of a cell transmission model and macroscopic fundamental diagram: network aggregation for dynamic traffic models. Transport. Res. Part C 55, 298–309.